Fine structure mediated magnetic response of trion valley polarization in monolayer WSe_2

Yalin Ma,[1,*] Qingxuan Wang,[1,*] Shixuan Han,[1] Fanyao Qu,[2] and Jiyong Fu[1,2,†]
[1]*Department of Physics, Qufu Normal University, 273165 Qufu, Shandong, China*
[2]*Instituto de Física, Universidade de Brasília, Brasília-DF 70919-970, Brazil*

(Received 15 June 2021; revised 11 October 2021; accepted 4 November 2021; published 19 November 2021)

We construct a valley dynamics model, involving both bright and dark excitonic states, to determine magneto-optical properties of excitons and singlet and triplet trions (charged excitons), in monolayer WSe_2 subjected to magnetic fields. Our computed excitonic peak energy and valley Zeeman splitting, which are essential for the magnetic-field-associated valley dynamics, in great agreement with experimental data by Lyons *et al.* [Nat. Commun. **10**, 2330 (2019)]. In addition, we find that the valley polarizations of excitons and trions respectively exhibit the "X"- and "V"-shape dependence on magnetic field, consistent with experimental measurements by Aivazian *et al.* [Nat. Phys. **11**, 148 (2015)]. Remarkably, beyond available experimental measurements, our theory predicts an X-V shape conversion and even a new paradigm more than the X and V shapes, which depend on the trion fine structure arising from exchange interactions and involving a magnetic *swap* of ground states between singlet and triplet trions. Our results are helpful for elucidating recent experimental data about the valley-degeneracy-lifting-mediated valley dynamics of different trion species and should stimulate experiments probing relevant new magneto-optical features.

DOI: 10.1103/PhysRevB.104.195424

I. INTRODUCTION

Transition-metal dichalcogenide (TMDC) monolayers, as atomically thin semiconductors with the chemical formula MX_2 ($M =$ Mo, W; $X =$ S, Se, Te), have attracted intense research interest following the discovery of direct band gaps at the inequivalent K and K' valleys of the Brillouin zone [1–3]. The space-inversion asymmetry along with the spin-orbit interaction lead to valley-contrasting spin splittings, termed *spin-valley locking* [4], which is protected by time-reversal symmetry. This gives rise to a host of emerging novel phenomena in the context of valley physics, including optical generation of valley polarization [5,6], the valley Hall effect [2,4], and valley coherence [7–10]. Furthermore, owing to the two-dimensional (2D) spatial confinement and reduced dielectric screening as well as large electron and hole effective masses, TMDCs exhibit strong Coulomb interactions [11,12], favoring the formation of tightly bound electron-hole pairs, namely, excitons with remarkably large binding energy of hundreds of meV. Also, in the presence of additional charges, neutral excitons may further capture an extra charge to form a three-particle complex called a trion (charged exciton) with a binding energy of tens of meV [13–17]. Neutral and charged excitons may dominate the emission spectrum of monolayer TMDCs at low and elevated temperatures [18].

The unique *spin-valley-locked* band structure embraces rich spin and valley configurations for the carrier occupation, allowing for hosting not only bright excitonic states [19,20] but also optically inaccessible dark excitonic states [13,21–24]. Bright (X_b) and dark (X_d) excitons are split primarily by conduction-band spin-orbit splitting [25], with the lowest-lying excitonic states being optically dark in W-based monolayer TMDCs but optically bright in Mo-based ones [24].

Due to the presence of extra charge, trions possess more spin and valley configurations than excitons. The feature of trion emission depends on the characteristic of its constituent exciton; that is, when the excess electron is bound to the bright (dark) exciton, the negative trion is bright (dark) [26,27]. More specifically, a dark trion (X_d^-) is composed of a dark exciton in one valley and an extra electron in the other valley, while for bright trion the extra electron may reside in the same valley or in a different valley as compared with the photoexcited electron-hole pair, referring to the intravalley singlet (X_s^-) and intervalley triplet (X_t^-) states, respectively [see left three panels in Fig. 1(a)]. Because of the exchange interaction, an energetic splitting δ_{ex} (a few meV) between X_t^- and X_s^- occurs with the former having a higher energy (fine structure [28]) [Fig. 1(b)]. As the intervalley scattering of an extra charge involves both a large momentum transfer and spin flip, trions in general have long spin and valley lifetimes, greatly fascinating for valley control in spin-valleytronic applications [25,29].

Similar to the real spin and atomic angular momentum, the valley pseudospin also has a magnetic moment, enabling control of the valley degree of freedom via magnetic field B [6,20]. The B field breaks time-reversal symmetry and causes opposite energy shifts in the K and K' valleys [6], referring to valley Zeeman effect—a valley analog of the spin Zeeman effect. As a direct consequence of valley selective optical transition rule [4], the valley Zeeman effect is imaged by spectral splitting between circularly polarized magneto-photoluminescence (PL) peaks with distinct helicity and greatly affects valley polarization (VP). Generating and manipulating VP is a critical step towards valleytronic

*These authors contributed equally to this work.
†yongjf@qfnu.edu.cn

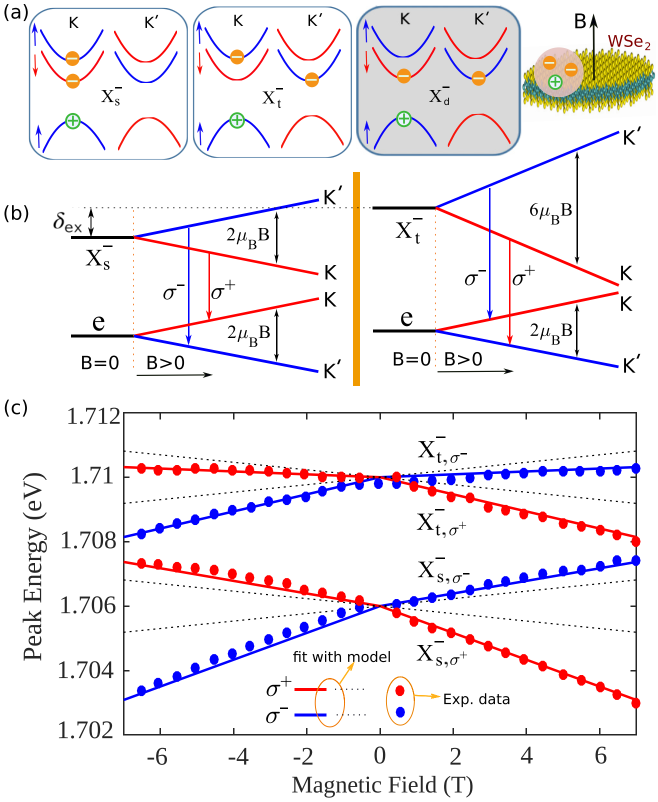

FIG. 1. (a) Illustration of spin and valley configurations for singlet (X_s^-) and triplet (X_t^-) bright trions and dark (X_d^-) trions comprising two electrons and a hole as well as a schematic of monolayer WSe_2 hosting three-particle complexes (trions) subjected to a perpendicular magnetic field. The blue (red) lines denote bands with up (down) electron spin, also indicated by the up (down) arrows. (b) Schematic of valley Zeeman splitting for X_s^- (left panel) and X_t^- (right panel), with the latter having an energy δ_{ex} higher than the former (fine structure) at zero field. Optical emissions featuring the dichroism paradigm are indicated by red and blue arrows for σ^+ and σ^- polarizations, respectively. (c) Peak energies of X_t^- and X_s^- under laser excitation of circularly polarized light with different helicities as functions of magnetic field. The circular markers refer to experimental data of Ref. [30] and the curves are obtained from theoretical simulation, where the solid (red; blue) and dotted (black) curves refer to the peak energy with and without contributions from the Berry-curvature-associated magnetic moment of the trion (initial state) and from the recoil effect of the additional electron (final state), respectively. In panel (c), we adopt the singlet-triplet splitting energy at $B = 0$ equal to 4 meV, which is determined via photoluminescence measurements in Ref. [30], to fit the data therein.

applications. Recently, a number of experimental measurements about magneto-valley dynamics of different trion species in monolayer TMDCs have been performed [6,30–33], whereas a detailed theoretical exploration is lagging, leading to the underlying physics remaining elusive.

Here we construct a model which takes into account both bright and dark excitonic states and determine the magneto-optical properties of excitons and singlet and triplet trions in monolayer WSe_2 subjected to a magnetic field [see right-most panel of Fig. 1(a)]. We compute the excitonic peak energy and valley Zeeman splitting under the laser excitation of σ^+ and σ^- circularly polarized light fields, referring to the optical response in the K and K' valleys (dichroism paradigm [4]), respectively, in strong agreement with the experimental data of Lyons *et al.* [30] [Fig. 1(c)]. Having energetic responses of excitonic states to magnetic field at hand, we then determine the magneto-PL and VP. We reveal that the exciton and trion VPs exhibit the X- and V-shape dependence on magnetic field, respectively, consistent with experimental measurements by Aivazian *et al.* [6] [Figs. 3(d) and 4(f)]. Remarkably, beyond the current experimental measurements, for the trion VP our calculation also indicates an X-V shape conversion and even a new paradigm more than the X and V shapes, depending on the fine structure of trions (Fig. 5). The magnetic response of PL with distinct contributions from singlet and triplet trion states as well as the effect of dark excitonic states is also discussed. Our results are helpful for elucidating recent experimental data about the valley-Zeeman-effect-mediated valley dynamics of different trion species and should stimulate experiments probing new magneto-optical features.

The rest of the paper is organized as follows: In Sec. II, we present our theoretical framework resolving the valley dynamics of excitons and trions with both bright and dark states in monolayer TMDCs subjected to magnetic field. First, we discuss the spin and valley configurations of excitons and trions and then determine the energies of relevant excitonic states which are essential for thermal excitation affecting the valley dynamics. To proceed in a systematic way, we first consider the scenario at zero magnetic field and then incorporate the magnetic response. Second, we take into account the relevant radiative and nonradiative scattering and relaxation channels and build up a set of coupled rate equations to describe magneto-valley dynamics. In Sec. III, by taking WSe_2 monolayer as a model system, we discuss our numerical outcome for magneto-optical properties of excitons and trions. A comparison with experimental data is also made. We summarize our main findings in Sec. IV.

II. THEORETICAL FRAMEWORK

The spin-orbit (SO) coupling lifts spin degeneracy and gives rise to a spin-polarized electronic band structure around the K and K' points in the Brillouin zone for both conduction and valence bands [2,4,34,35]. The spin splitting of the valence band, which primarily arises from the transition metal $d_{x^2-y^2}$ and d_{xy} orbitals, is around hundreds of meV [36], far greater than that of conduction band, which ranges from several to tens of meV [35] and is dominated by the d_{z^2} orbital of the transition-metal atom and $p_{x,y}$ orbitals of the chalcogen atom. As a consequence, optically allowed interband transitions from the two spin states of the valence band are well separated, referring to A and B excitons [37]. This allows us to develop a theory within only three bands, consisting of one spin-branch of valence band with higher energy and both spin branches of the conduction band, i.e., for A excitons only [38].

Band-structure calculations suggest that the spin states of the conduction band may have opposite orderings in energy [35], depending on transition-metal atoms, as opposed to that of valence band. This leads to the lowest-energy transition (ground state) being optically bright (spin allowed) in MoX_2 and optically dark (spin forbidden) in WX_2 [35].

The nature of dark excitation has been theoretically unraveled with the help of *ab initio* many-body calculations [39]. Also, the existence of dark excitons has been experimentally identified through time-resolved PL spectroscopy [27], magneto-PL [40,41] and infrared spectroscopy [42,43]. Very recently, direct observations of gate-tunable dark trions have also been demonstrated [26,44].

Beside bright excitonic states, optically inaccessible dark states also play a profound role in the valley dynamics. On the one hand, optically dark states could provide a robust reservoir for valley polarization [22,45], suppressing the valley relaxation [46]; on the other hand, dark channels could quench the light emission by *absorbing* bright states [27,42,43,47]. Therefore, to more accurately reveal magneto-optical properties in monolayer TMDCs, it is necessary to account for in the model both bright and dark states with distinct spin and valley configurations.

A. Spin and valley configurations of excitons and trions: Both bright and dark states

Below we restrict our focus to monolayer WSe_2, which can be extended to other W-based and even Mo-based TMDC materials. Bright (X_b) and dark (X_d) excitons are split primarily by conduction-band spin-orbit splitting [35]. Bright trions include the intravalley singlet state (X_s^-) consisting of carriers (three-particle complex) located within a single valley and the intervalley triplet state (X_t^-) comprising an electron-hole pair in one valley and an additional electron in the other valley [Fig. 1(a)]. An energetic splitting δ_{ex} between X_s^- and X_t^- emerges due to the electron-hole exchange interaction, with $\delta_{ex} \approx 6$ meV in monolayer WSe_2, giving rise to the fine structure of trions [14] [Fig. 1(b)]. A dark trion X_d^- is composed of a dark exciton in one valley and an extra electron in the other valley [Fig. 1(a)]. Note that, in Fig. 1(a), we only illustrates the spin and valley contributions of different trion species with the electron-hole pairs residing in the K valley. Clearly, there also exists the other three configurations (counterparts) with the electron-hole pairs being accommodated in the K' valley (not shown), since the two valleys are related to each other by time-reversal symmetry. Below we determine the energy of relevant excitonic states with distinct spin and valley configurations.

B. Energy of excitons and trions

We first compute the energy of excitonic states at zero field. Then, we determine the corresponding valley Zeeman shift under the impact of magnetic fields.

1. Zero magnetic field

Based on the two-band model proposed by Xiao *et al.* [4], one can determine the energy of excitonic states in the K and K' valleys by resorting to the band-edge energies of independent electrons and holes (single-particle picture). Then, we take into account many-body interactions to determine the binding energy of excitonic states by solving the Bethe-Salpeter equation (BSE) [48–51], for which the two-particle exciton state reads $\Psi_n = \sum_{c,v,\mathbf{k}} J^{(n)}_{c,v,\mathbf{k}} |v\mathbf{k} \rightarrow c\mathbf{k}\rangle$, where c (v) denotes the conduction (valence) band, $\mathbf{k}$ is the wave vector, and J stands for the BSE expansion coefficient. To more accurately determine the single-particle states used for evaluating many-body corrections as well as electronic band structures of monolayer WSe_2, we adopt an eleven-band tight-binding (TB) model of five d orbitals of W atoms and six p orbitals of two Se atoms and take into account the second-nearest-neighbor hopping terms [52]. For more details about single-particle and many-body calculations, see Refs. [48–51] as well as our recent works [1,53,54].

Now we are ready to write down the energy of an electron ($E^{c,\tau}_{S_e}$) and hole ($E^{v,\tau}_{S_h}$) at the conduction- and valence-band edges,

$$E^{c,\tau}_{S_e} = E_g + \tau S_e \Delta_c, \tag{1}$$

and

$$E^{v,\tau}_{S_h} = -\tau S_h \Delta_v, \tag{2}$$

respectively, where E_g is the fundamental band gap, τ represents the valley index for K ($\tau = 1$) and K' ($\tau = -1$) valleys, $S_{e(h)}$ denotes the spin index with $S_{e(h)} = 1/2$ for spin-up ($\uparrow$) and $S_{e(h)} = -1/2$ for spin-down ($\downarrow$) states of electrons (holes), and $\Delta_{c(v)}$ indicates the spin-orbit splitting energy in the conduction (valence) band. With the help of Eqs. (1) and (2) as well as the many-body calculation via solving the BSE [1,53], the energy of bright excitonic states at zero field is written as

$$\begin{aligned} E^{\tau}_{X_b}(B=0) &= E^{c,\tau}_{S_e} + E^{v,\tau}_{S_h} - \langle V^{\tau}_{e-h}\rangle \\ &= E_g + \tfrac{1}{2}\Delta_c - \tfrac{1}{2}\Delta_v - V_{X_b}, \end{aligned} \tag{3}$$

$$\begin{aligned} E^{\tau}_{X_s^-}(B=0) &= E^{c,\tau}_{S_e} + E^{c,\tau}_{-S_e} + E^{v,\tau}_{S_h} - \langle V^{\tau}_{e-e-h}\rangle \\ &= 2E_g - \tfrac{1}{2}\Delta_v - V_{X_b} - V_{X_s^-}, \end{aligned} \tag{4}$$

$$\begin{aligned} E^{\tau}_{X_t^-}(B=0) &= E^{c,\tau}_{S_e} + E^{c,-\tau}_{S_e} + E^{v,\tau}_{S_h} - \langle V^{\tau}_{e-e-h}\rangle \\ &= 2E_g - \tfrac{1}{2}\Delta_v - V_{X_b} - V_{X_t^-}, \end{aligned} \tag{5}$$

where $\langle V^{\tau}_{e-h}\rangle$ and $\langle V^{\tau}_{e-e-h}\rangle$ represent the many-body corrections, i.e., averaged expectation values obtained from the BSE, with the former $\langle V^{\tau}_{e-h}\rangle = V_{X_b}$ referring to the exciton binding energy. Regarding the latter $\langle V^{\tau}_{e-e-h}\rangle = V_{X_b} + V_{X_s^-}$ and $V_{X_b} + V_{X_t^-}$ for the singlet and triplet trions, respectively, we have as usual defined $V_{X_s^-}$ ($V_{X_t^-}$) the binding energy of singlet (triplet) trions by taking the exciton binding energy as a reference. With the help of the BSE, we obtain $V_{X_b} =$ 450 meV, consistent with experimental reports about the exciton binding energy in WSe_2 on SiO_2 substrates, which are about 500 meV [17,55–57]. And, for trions, we obtain $V_{X_s^-} = 27$ meV, and $V_{X_t^-} = 21$ meV, with $V_{X_s^-} - V_{X_t^-} = 6$ meV determining the fine structure of trions. These values are also consistent with experimental reports about the excitonic emission spectrum [41,44,57,58]. For more energy parameters used in our simulation, see Table I.

It is worth noting that the binding energies of trions are calculated using the BSE containing three-body terms [48,49], i.e., two electrons and one hole for negatively charged excitons. Specifically, the trion states are constructed as $|X^-, \mathbf{Q}\rangle = \sum_{v,c_1,c_2} A^{\mathbf{Q}}_{v,c_1,c_2} |v, c_1, c_2\rangle$, where $\mathbf{Q}$ is the total momentum of trion states and $|v, c_1, c_2\rangle = \hat{a}^{\dagger}_{c_2}\hat{a}^{\dagger}_{c_1}\hat{a}_v|0\rangle$, with $|0\rangle$ standing for the ground state of an N-electron system and

TABLE I. Relevant energy parameters for monolayer WSe_2 (Sec. II B 1). We consider the band gap $E_g = 2.2$ eV [56,79] and the conduction- and valence-band SO splitting $\Delta_c = 35$ [61,78] and $\Delta_v = 460$ meV [4,61,78]. The binding energies (in meV) of excitonic states are listed below, including bright exciton (X_b) and singlet (X_s^-) and triplet (X_t^-) trions as well as dark exciton (X_d) and trion (X_d^-).

	V_{X_b}	$V_{X_s^-}$	$V_{X_t^-}$	V_{X_d}	$V_{X_d^-}$
Binding energy[a]	450	27	21	433	15

[a]From our two-particle (exciton) and three-particle (trion) BSE calculations, close to the values in Refs. [17,55–57,80] for excitons and in Refs. [41,44,57,58] for trions.

the index v (c_1 and c_2) referring to occupied valence (empty conduction) states.

2. Valley Zeeman shift

The main effect of an out-of-plane magnetic field (Faraday geometry) on monolayer TMDCs is to break time reversal symmetry and further lifts the valley degeneracy. The energy shift mainly comprises three contributions from the spin magnetic moment, valley pseudospin magnetic moment, and transition-metal atomic magnetic moment [6]. The spin and valley contributions respectively read $\Delta_s = g_s s_z \mu_B B$ and $\Delta_v = g_v \tau \mu_B B$, where we have defined μ_B as the Bohr magneton, $g_s = 2$ as the spin g factor, $s_z = \pm 1/2$ as denoting the up and down spins, and $g_v = m_0/m^*$ as the valley g factor with m_0 (m^*) the bare (effective) mass for electrons and holes [6]. Here we have assumed that the valley g factor $g_v \approx 2$ is the same for conduction and valence bands, which is true up to leading order in the $\mathbf{k}\cdot\mathbf{p}$ approximation for band-edge carriers [6]. Furthermore, the atomic contribution is written $\Delta_a = g_a \tau \mu_B B$, with g_a the magnetic quantum number of atomic orbitals. As a first approximation, this contribution does not affect the conduction-band edges which are mainly composed of d orbitals with $g_a = 0$, while it does shift the valence-band edges which primarily consist of d orbitals with $g_a = 2$.

In addition to the above band-edge shifts of the single-particle band structure, the exchange induced modification of the trion dispersion leads to the trion states with center-of-mass momentum $\pm K$ carrying a large Berry curvature $\Omega(k)$, which is accompanied by a contribution to the magnetic moment $\mu(k) = (e/2\hbar)\Omega(k)\delta_{ex}$ for $k \approx \pm K$, with $\Omega(k) \sim 10^{-4}$ Å^2 [20,30]. Note that this additional contribution to the magnetic moment exists only in the initial trion state of optical emission, giving rise to a larger splitting of the peak energy for laser excitation with different circular polarizations as compared with that of excitons [58]. Clearly, the Berry-curvature associated μ yields an extra energy shift $\Delta_b = (1/2)g_\Omega \mu_B B$ for trions, with the related Landé factor $g_\Omega = (m_e/\hbar^2)\Omega\delta_{ex}$. We consider $g_\Omega \approx 4$ in our WSe_2 monolayer [30]. We should emphasize that the Berry curvature $\Omega(k)$ of trion states due to the fine structure arising from the electron-hole exchange interaction that is introduced above is in contrast with that of individual conduction (or valence) bands for band-edge electrons [4,59,60], with the former around two or three orders of magnitude larger than the latter [4,20,30].

With all these considerations, for $B > 0$ it follows straightforwardly the field-dependent energy changes of excitons and trions,

$$\Delta E^\tau_{X_b}(B) = -\Delta_a, \tag{6}$$

$$\Delta E^\tau_{X_s^-}(B) = \Delta_v - \Delta_a - \Delta_s - \Delta_b, \tag{7}$$

$$\Delta E^\tau_{X_t^-}(B) = \Delta_s - \Delta_a - \Delta_v - \Delta_b, \tag{8}$$

and then the corresponding valley Zeeman splitting energy, with $\Delta E^{KK'}_{X_b} = -2\Delta_a$, $\Delta E^{KK'}_{X_s^-} = 2(\Delta_v - \Delta_a - \Delta_s - \Delta_b)$, and $\Delta E^{KK'}_{X_t^-} = 2(\Delta_s - \Delta_a - \Delta_v - \Delta_b)$. Clearly, the equality $\Delta E^\tau_{X_b}(-B) = \Delta E^{-\tau}_{X_b}(B)$ for excitons holds because of magnetic nature of the valley degree of freedom, similarly for trions $\Delta E^\tau_{X_t^-}(-B) = \Delta E^{-\tau}_{X_t^-}(B)$ and $\Delta E^\tau_{X_s^-}(-B) = \Delta E^{-\tau}_{X_s^-}(B)$.

As a remark, here we decompose the contribution of orbital angular momentum to magnetic moment into the atomic (intracellular) and valley (intercellular) constituents, referring to the g factors of g_a and g_v, respectively, in the way that is widely adopted in literature [6,30,47,61,62]. Note that this treatment of orbital angular momentum for monolayer WSe_2 is consistent with more rigorous considerations dealing with valley and atomic contributions in a unified way through *ab initio* calculations [63–66], which are also verified by recent experimental measurements [66–68]. On the other hand, for van der Waals heterostructures of TMDCs, in which the g factors may even be strongly stacking dependent [64], one should resort to more rigorous way of *ab initio* calculations for determining the valley Zeeman effect.

3. Excitonic peak energy

The excitonic peak energy is defined as the energy difference between the initial and final states. Equations (3)–(8) define the energy of excitons and trions (initial state), involving the zero-field energy [Eqs. (3)–(5)] and an energy modification due to the valley Zeeman effect [Eqs. (6)–(8)]. Regarding the final state, for excitons the electron-hole pair just recombines radiatively, while for trions after the recombination of electron-hole pairs there is still an extra electron left, which may involve the recoil effect and Landau-level quantization [30]. With all these considerations, we have the peak energy for excitons and singlet and triplet trions,

$$\Delta E^\tau_{h\nu}(X_b) = E_g + \tfrac{1}{2}\Delta_c - \tfrac{1}{2}\Delta_v - V_{X_b} - \Delta_a, \tag{9}$$

$$\Delta E^\tau_{h\nu}(X_s^-) = E_g - \tfrac{1}{2}\Delta_v + \tfrac{1}{2}\Delta_c - V_{X_b} - V_{X_s^-} - \Delta_a - \Delta_b - \Delta_e - \Delta_l, \tag{10}$$

$$\Delta E^\tau_{h\nu}(X_t^-) = E_g - \tfrac{1}{2}\Delta_v + \tfrac{1}{2}\Delta_c - V_{X_b} - V_{X_t^-} - \Delta_a - \Delta_b + \Delta_e - \Delta_l, \tag{11}$$

in which for the peak energy of trions we have defined $\Delta_l = (1/2)g_l\mu_B B$ as the Landau-level contribution of the final-state electron [30]. Note that the Landau-level quantization for the initial trion state has been neglected thanks to its much larger effective mass than the electron. Also, with the excess electron in the K (K') valley, the trions have the center-of-mass wave vector $Q_{X_{s,t}^-} \equiv K + k$ ($Q_{X_{s,t}^-} \equiv -K + k$),

TABLE II. Relevant g factors associated with the valley Zeeman effect (Secs. II B 2 and II B 3), including the contributions from the spin (g_s), valley (g_v), and atomic (g_a) constituents as well as the contributions from the recoil effect (g_e), Landau level (g_l), and trion Berry curvature (g_Ω), with g_Ω depending on the fine structure of trions induced by the electron-hole exchange interaction.

	g_s	g_v	g_a	g_e	g_l	g_Ω
g factor[a]	2[b]	2[b]	2[b]	2.6[c]	4[c]	4[d]

[a]Here the contribution of orbital angular momentum to magnetic moment is decomposed into the atomic (intracellular) and valley (intercellular) constituents, referring to the g factors of g_a and g_v, respectively [6,30,47,61,62]. This is consistent with recent more rigorous considerations treating the two constituent contributions in a unified way through *ab initio* calculations for monolayer WSe_2 [63–66], which are also verified by experimental measurements [66–68].
[b]From Refs. [6,47].
[c]From Refs. [30].
[d]From Refs. [20,28,30].

in favor of the recombination of trions as the recoil of the excess electron facilitates the momentum conservation [20]. Here the recoil effect of the final-state electron is taken into account through $\Delta_e = (1/2)g_e\mu_B B$ [30]. Based on the experimental reports of Ref. [30], we consider $g_l = 4$ and $g_e = 2.6$ in the WSe_2 monolayer. Note that here $g_e = 2.6$ characterizes the valley Zeeman splitting of the lower spin branch of conduction band (c_1 band), and hence is twice the value of the band g factor [i.e., $g(c_1)$], namely, corresponding to $g(c_1) = 1.3$, close to the value of 0.9 demonstrated in recent studies through either *ab initio* calculations [63] or experimental measurements [67,68]. All relevant g factors are summarized in Table II.

C. Exciton and trion valley dynamics under magnetic field

To explore the effect of valley Zeeman shifts described in Sec. II B 2 on the magneto-optical properties of excitons and trions in a WSe_2 monolayer, we resort to a set of coupled rate equations describing the valley dynamics. And we take into account all the relevant transition and scattering channels of both intra- and intervalley kinds, as illustrated in Fig. 2, among excitonic states including the bright (X_b) and dark (X_d) excitons and bright (singlet X_s^-; triplet X_t^-) and dark (X_d^-) trions in the K and K' valleys.

1. Intravalley scattering channels

We first look at the intravalley case. As the K and K' valleys are related to each other by time-reversal symmetry, there is a one-to-one correspondence between the two valleys for either the excitonic states or the scattering channels. Hence, we only focus on the K valley (left panel of Fig. 2) [69], in which the bright excitons X_b are photocreated under the laser exciton of σ^+ circularly polarized light with the generation rate g, see the solid red (up) arrow. The solid red, blue, and green (down) arrows indicate that the bright states X_b, X_t^-, and X_s^- decay radiatively, with the lifetime of τ_x, τ_t, and τ_s, respectively. Analogously, the dark states of X_d and X_d^-, which separately have the lifetime τ_d and τ_{td}, undergo the nonradiative decay to the ground states, as indicated by the solid gray (down) arrows. In Table III, we list all relevant excitonic lifetimes.

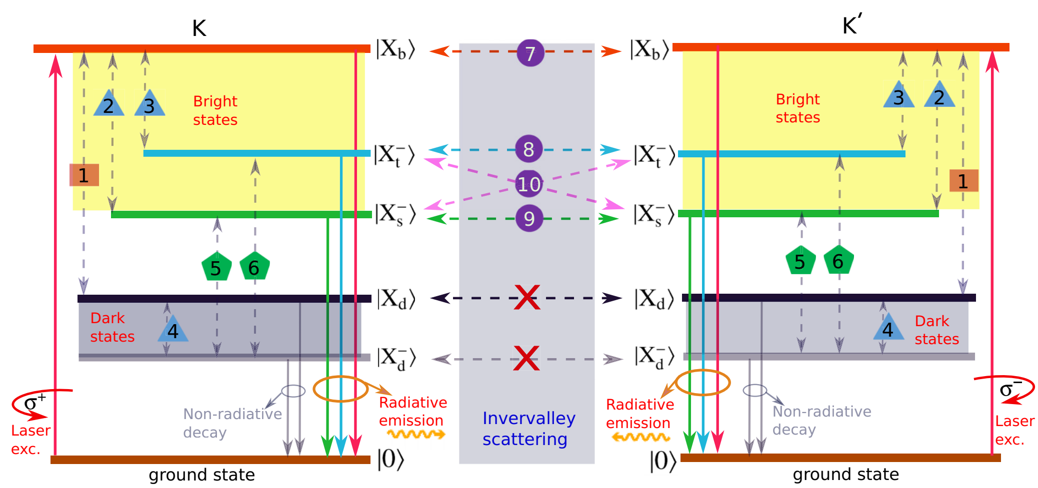

FIG. 2. (a) Schematic of the intra- and intervalley relaxation and scattering channels involving the bright states of X_b, X_t^-, and X_s^- and dark states of X_d and X_d^-, under the circularly polarized σ^+ (σ^-) pumping light for the K-valley (K'-valley) excitation. The solid up (red) arrows denote generation of excitons by laser excitation, and the solid down arrows indicate the radiative emission of X_b (red), X_t^- (blue), and X_s^- (green) as well as the nonradiative decay of X_d and X_d^- (gray). The dotted arrows indicate nonradiative intra- and intervalley scatterings among excitonic states, which are labeled by the numbers 1–6 for the intravalley and 7–10 for the intervalley relaxation channels. Regarding the former intravalley scenario, label 1 represents scattering processes only for excitons, labels 2–4 between excitons and trions, and labels 5 and 6 only for trions; for the latter intervalley case, scattering channels between dark states are greatly suppressed [21] and hence is ignored. The double arrows for each scattering channel (e.g., channel 1) indicates *reversible* processes of down- and up-conversions, with the former energetically favorable and the latter not.

TABLE III. Relevant lifetimes (in ps) for X_b (τ_x), X_s^- (τ_s), X_t^- (τ_t), X_d (τ_d), and X_d^- (τ_{td}) (Secs. II C 1 and II C 3) at $T = 30$ K. In the table, for τ_x, $\tau_0 = \tau(T = 0) = 0.7$ ps and $\alpha = 0.15$ ps/K [54,76]; for $\tau_{s,t}$, $\beta = 100$ ps K and $\gamma = 0.001$ ps K^{-2} [38,54,77].

	τ_x	τ_s	τ_t	τ_d	τ_{td}
Lifetime	$\alpha T + \tau_0$	$\beta/T + \gamma T^2$	$\beta/T + \gamma T^2$	150[a]	230[b]

[a]From Ref. [81].
[b]From Ref. [41].

TABLE IV. Relevant intravalley scattering rates (in ps^{-1}) (Secs. II C 1 and II C 3). In the table, the trion formation rate f and dissociation rate d depend on electron concentration n_e [54,82,83], the value of which is $n_e = 2 \times 10^{11}$ cm^{-2}.

	Γ_1	f	d_i ($i = 2$–4)	Γ_5	Γ_6
Intravalley	1[a]	$2.45 \times 10^3 n_e/T$	$5 \times 10^{-4} u_i/n_e$	0.75[a]	1[a]

[a]From Refs. [25,54].

In addition to the aforementioned optical transitions involving the excitonic states and ground state, there also exists intravalley relaxation and scattering channels among excitonic states with distinct spin and valley configurations. To facilitate our discussions, we classify these scattering channels into three groups, with group I only for neutral excitons, group II between neutral and charged excitons, and group III only for charged excitons.

In the first group, the scatterings contain a *reversible* relaxation channel of down- and up-conversions, as indicated by the double-arrow process labeled by 1, with the former energetically favorable and the latter not. In this process, a bright exciton can relax nonradiatively to a dark exciton through the spin-flipping process with the scattering rate Γ_1. In turn, the exciton in the dark (low-energy) state can be thermo-excited to the bright (high-energy) state with the transition rate weighted by a Boltzmann factor $u_1 = \exp(-\Delta E_{bd}/k_B T)$. Here we have defined ΔE_{bd} as the energy separation between bright and dark excitons, k_B as the Boltzmann constant, and T as the temperature.

In group II, as labeled by 2, 3, and 4, the scattering channels refer to the formation and dissociation of X_s^-, X_t^-, and X_d^-, respectively. Namely, the bright and dark excitons can capture an additional electron to form charged three-particle complexes, i.e., triplet (X_t^-), singlet (X_s^-) trions, and dark trions (X_d^-). The formation rate of trions may depend linearly on the electron density n_e and is inversely proportional to temperature, with the form $f = 2.45 \times 10^3 n_e/T$ nm^2 K ps^{-1} [54]. As for the reversed (dissociation) process, which refers to the up-conversion process, the scattering rate clearly decreases with n_e and increases with growing temperature and is described by $d_i = 5 \times 10^{-4} u_i/n_e$ nm^{-2} ps^{-1} [54]. Here the subscript i represents the corresponding scattering channel, with $i = 2, 3, 4$ for X_s^-, X_t^-, and X_d^-, respectively. Also, $u_i = \exp(-\Delta E_i/k_B T)$ refers to the Boltzmann factor characterizing the up-conversion process, with ΔE_i the energy separation between the ith trion state and the corresponding exciton state after the trion dissociation. Note that here we have assumed that different trion states of X_s^-, X_t^-, and X_d^- have the same formation rate f, and the distinction of their dissociation rates is encoded in the Boltzmann factor which is energy dependent.

Group III consists of scattering channels 5 and 6 referring to the intravalley relaxation processes between bright and dark trions, with 5 (6) denoting the reversible channel between X_s^- (X_t^-) and X_d^-. The scatterings from X_s^- (X_t^-) to X_d^- are energetically favorable with the scattering rates described by Γ_5 (Γ_6). Regarding the backward-scattering processes, they are energetically unfavorable and the scattering rates are determined by $\Gamma_5 u_5$ and $\Gamma_6 u_6$, where the Boltzmann distributions $u_5 = \exp(-\Delta E_{sd}/k_B T)$ and $u_6 = \exp(-\Delta E_{td}/k_B T)$ act as weighting parameters to the forward-scattering rates and determine the thermalized excitation, with ΔE_{sd} (ΔE_{td}) the energy separation between singlet (triplet) and dark trions. The relevant intravalley scattering rates are summarized in Table IV.

2. Intervalley scattering channels

In the middle panel of Fig. 2, we illustrate the intervalley relaxation and scattering channels, as indicated by the labels 7–10. Process 7 represents the scattering channel for bright excitons with relaxation rate $\alpha_x^{KK'}$, which is induced by the electron-hole exchange interaction through the Maialle-Silva-Sham (MSS) mechanism [21,70,71]. In this process, electrons in the conduction band of the K valley and valence band in the K' valley are scattered to the valence band in the K valley and conduction band in the K' valley, respectively. Alternatively, this process can also be thought as the result of virtual recombination of a bright exciton in the K (K') valley and generation in the K' (K) valley. Similarly, the intervalley scattering also exists for triplet (process 8) and singlet (process 9) trions with the relaxation rates $\alpha_t^{KK'}$ and $\alpha_s^{KK'}$, respectively. As compared with excitons, for which $1/\alpha_x^{KK'} \approx 1$ ps [29], the intervalley scattering of trions may have much longer relaxation time, with $1/\alpha_t^{KK'}$ and $1/\alpha_s^{KK'}$ more than 25 ps in monolayer WSe_2 [29], because the scattering involves the transfer of a single electron from one valley to the other [29,72], accompanied by a simultaneous large momentum transfer and spin flip.

In addition to the intervalley transfer of excitonic states of the same type, an intervalley scattering can also transfer the singlet (triplet) trion state in the K valley into the triplet (singlet) state in the K' valley, and vice versa, with the relaxation rate $\alpha_{st}^{KK'}$, as illustrated by the process 10. Note that the intervalley scattering between singlet and triplet states does not involve the spin flip and thus is much more favorable than process 9 between singlet and singlet states and process 8 between triplet and triplet states [29,72].

Regarding the intervalley scattering of dark states, i.e., X_d and X_d^-, the process is greatly suppressed as a consequence of vanishing matrix elements for both the intervalley long-range and short-range exchange interactions [20], and hence is ignored in our model. In Table V, we list relevant intervalley scattering rates.

3. Valley dynamics of excitons and trions: Coupled rate equations

Armed with the aforementioned transition and scattering channels of both intra- and intervalley types, we are ready

TABLE V. Relevant intervalley scattering rates (in ps^{-1}) (Secs. II C 2 and II C 3). The field-dependent scattering rates [see Eqs. (17) and (18)] are obtained by fitting our simulation to experimental data of Refs. [6,30].

	$\alpha_x^{KK'}$	$\alpha_{st}^{KK'}$	$\alpha_s^{KK'}$	$\alpha_t^{KK'}$
Intervalley	Eq. (17)	Eq. (18)	30[a]	30[a]

[a]For $\alpha_s^{KK'}$ and $\alpha_t^{KK'}$, our fitting shows that they are essentially independent of magnetic field as a result of long intervalley scattering time due to suppressed valley relaxation, which is also consistent with experimental measurements [29].

to write down a set of coupled rate equations describing the valley dynamics of excitons and trions in the K valley,

$$\frac{dn_b}{dt} = g - \frac{n_b}{\tau_x} - \Gamma_1 n_b + \Gamma_1 u_1 n_d - 2fn_b + d_2 n_s^- + d_3 n_t^- + \alpha_x^{K'K} n_b' - \alpha_x^{KK'} n_b, \tag{12}$$

$$\frac{dn_d}{dt} = -\frac{n_d}{\tau_{xd}} - \Gamma_1 u_1 n_d + \Gamma_1 n_b - fn_d + d_4 n_d^-, \tag{13}$$

$$\frac{dn_t^-}{dt} = -\frac{n_t^-}{\tau_t} + fn_b - d_3 n_t^- - \Gamma_6 n_t^- + \Gamma_6 u_6 n_d^- + \alpha_{st}^{K'K} u_{10} n_s^{-\prime} - \alpha_{st}^{KK'} n_t^- + \alpha_t^{K'K} n_t^{-\prime} - \alpha_t^{KK'} n_t^-, \tag{14}$$

$$\frac{dn_s^-}{dt} = -\frac{n_s^-}{\tau_s} + fn_b - d_2 n_s^- - \Gamma_5 n_s^- + \Gamma_5 u_5 n_d^- + \alpha_{st}^{K'K} n_t^{-\prime} - \alpha_{st}^{KK'} n_s^- + \alpha_s^{K'K} n_s^{-\prime} - \alpha_s^{KK'} n_s^-, \tag{15}$$

$$\frac{dn_d^-}{dt} = -\frac{n_d^-}{\tau_{td}} + fn_d - d_4 n_d^- + \Gamma_5 n_s^- - \Gamma_5 u_5 n_d^- + \Gamma_6 n_t^- - \Gamma_6 u_6 n_d^-, \tag{16}$$

where n_b, n_d, n_s^-, n_t^-, and n_d^- are the K-valley concentrations of X_b, X_d, X_s^-, X_t^-, and X_d^-, respectively. All quantities labeled by a superscript "$\prime$" (e.g., n_b') on the right-hand side of the equations represent the corresponding counterparts of the K' valley, indicating the coupling of the two valleys. The valley dynamics of excitonic states in the K' valley is connected to that in the K valley through time-reversal symmetry.

Referring to Eqs. (12)–(16), we should emphasize two points. First, for the intervalley scattering rates $\alpha^{KK'}$ ($\alpha^{K'K}$), we have resorted to the superscript "KK'" ($K'K$) for identifying the intervalley scattering of relevant excitonic states from the K (K') to the K' (K) valleys, with $\alpha^{KK'}$ ($\alpha^{K'K}$) is energetically favorable when B is greater (less) than zero. Second, all the involved Boltzmann factors in the thermo-excited process depend not only on the temperature but also on the magnetic field. Specifically, the magnetic field modifies the energy separation through Zeeman shifts, which combine with the temperature determine thermal equilibrium processes between excitonic states.

We compute the PL intensity for each individual excitonic states via n/τ [73], where n and τ *generally* represent the excitonic concentrations and the corresponding recombination times appearing in the above rate equations. By directly solving the set of coupled rate equations, one can obtain the time evolution of PL [38]. By setting the left-hand side of the rate equations equal to zero, i.e., $dn/dt = 0$, we determine the steady-state solution for the PL intensity. The valley polarization η is associated with the distinction of PL intensity between the K and K' valleys, i.e., $\eta^i = [PL^i(K) - PL^i(K')]/[PL^i(K) + PL^i(K')]$ [74,75], with the superscript i standing for excitonic states.

III. RESULTS AND DISCUSSION

We first introduce our system and the relevant parameters adopted. From fitting our model to experimental data, we also extract the intervalley relaxation times of excitonic states as well as the corresponding B-field dependence. Then we present our numerical outcome on valley dynamics of excitons and trions under the impact of magnetic field.

A. System and relevant parameters

In our numerical simulation, we consider monolayer WSe_2, which is in favor of hosting excitonic complexes of neutral and charged excitons [27]. The wavelength of excitation is 400 nm and the laser spot size is assumed to be 1 μm [27,45]. A Gaussian pulse duration of $\sigma = 44$ ps is adopted, $P = P_0 \exp[-4\ln(2)(t^2/\sigma^2)]$, with P_0 being the excitation fluence [27,45]. We consider the exciton generation rate $g \approx 1.87 \times 10^{-6}$ $nm^{-2}\,ps^{-1}$. The radiative decay time of bright excitons in general is temperature dependent and is written as $\tau_x = \alpha T + \tau_0$, where $\tau_0 = \tau(T=0) = 0.7$ ps and $\alpha = 0.15$ ps/K [54,76]. For bright trions, the radiative decay time reads $\tau_t = \beta/T + \gamma T^2$, with $\beta = 100$ ps K and $\gamma = 0.001$ ps K^{-2} [38,54,77]. Note that, since the difference between singlet and triplet-trion binding energies is only several meV, their dipole oscillator strengths are expected to be close. Also, in the case of low and intermediate free carrier concentrations, the trion radiative lifetime is mainly determined by that of its constituent bright exciton, which is the same for the singlet and triplet trions. Thus, we assume the same radiative lifetime for singlet and triplet trions, i.e., $\tau_s = \tau_t$, as is widely adopted in the literature [44,54]. Regarding the nonradiative decay of dark excitons and trions, we choose $\tau_{xd} = 150$ ps [54,77] and $\tau_{td} = 230$ ps [24,40], respectively.

The intravalley scattering channels among excitonic states contain relaxation processes 1–6, which are illustrated in Fig. 2. The bright-dark exciton scattering rate associated with the process 1 is chosen as $\Gamma_1 = 1$ ps^{-1}. The formation (f) and dissociation (d) rates of trions, which correspond to channels 2–4, depend on both the electron density and temperature, see Sec. II with the explicit form. Both the singlet and triplet (bright) trions *connect* with dark trions, and we take the corresponding scattering rates Γ_5 and Γ_6 equal to 0.75 and 1 ps^{-1} [25], respectively. At zero B field, the energy separation between singlet and triplet trions is $\delta_{ex} = 6$ meV and the bright-dark splitting energy $\Delta E_{bd} = 35$ meV is considered [25,78], unless stated otherwise. The temperature is 30 K [77].

As for intervalley relaxation channels [processes 7–10 in Fig. 2], a perpendicular magnetic field lifting valley degeneracy may affect the valley dynamics by modifying the intervalley relaxation time, which depends on the initial and final states of distinct valleys before and after scattering. Since the intervalley scattering is the key source leading to the valley depolarization, a field dependence of VP follows. Recently, the field effect on the valley polarization has been experimentally confirmed through polarization-resolved PL [6,41]. For neutral excitons, experimental data reveal that the VP under σ^+ and σ^- excitations as a function of magnetic field "crosses" at $B = 0$ and exhibits an X pattern. In contrast, the magnetic response of trion VP features a V pattern.

The X pattern of excitons can be understood as a consequence of the magnetic tuning of excitonic dispersion [6], which gives rise to *asymmetric* valley-conserving and valley-flipping exciton formation processes in the presence of a perpendicular magnetic field. The V pattern of trions may depend on the trion fine structure, which suppresses the intervalley relaxation and further protects the valley polarization for either sign of B.

Based on our model, by fitting the exciton and trion VPs *simultaneously* with the experimental data of Ref. [6], as shown in Figs. 3(d) for excitons and 4(f) trions, we observe a linear dependence of intervalley scattering times on B.

Under the laser excitation of σ^+ circularly polarized light, we obtain the following field-dependent intervalley scattering times for excitons:

$$\frac{1}{\alpha_{\mathrm{x}}^{KK'}} = \begin{cases} -0.02\ \mathrm{ps\,T^{-1}}B + 0.5\ \mathrm{ps} \text{ if } B \geqslant 0 \\ -0.06\ \mathrm{ps\,T^{-1}}B + 0.5\ \mathrm{ps} \text{ otherwise,} \end{cases} \tag{17}$$

and for trions of distinct types (i.e., singlet-triplet relaxation),

$$\frac{1}{\alpha_{\mathrm{st}}^{KK'}} = \begin{cases} -0.02\ \mathrm{ps\,T^{-1}}B + 0.6\ \mathrm{ps} \text{ if } B \geqslant 0 \\ -0.14\ \mathrm{ps\,T^{-1}}B + 0.6\ \mathrm{ps} \text{ otherwise.} \end{cases} \tag{18}$$

Note that the valley scattering time ($\approx$0.6 ps) at zero field that we extracted from fitting our model with experimental data agrees with recent reports in the literature [29]. Regarding the intervalley scattering between trions of the same types, i.e., singlet-singlet or triplet-triplet scattering, the relaxation time has been experimentally demonstrated to be more than 25 ps [29]. The suppressed valley relaxation is attributed to the *quenched* intervalley transfer of the extra charge of the trion, which involves a simultaneous spin flip and large momentum transfer. From our fitting, we reveal that $1/\alpha_{\mathrm{s}}^{KK'}$ and $1/\alpha_{\mathrm{t}}^{KK'}$ equal 30 ps, consistent with experimental measurements [29]. Also, we observe that $1/\alpha_{\mathrm{s}}^{KK'}$ $(1/\alpha_{\mathrm{t}}^{KK'})$ is essentially independent of magnetic field, as a result of long intervalley scattering time due to suppressed valley relaxation.

On the other hand, under the σ^- circularly polarized laser excitation, the B-field dependence of intervalley scattering times features opposite slopes to those described in Eqs. (17) and (18) for σ^+ polarization. This is attributed to the valley-dependent Zeeman splitting. In other words, following from the spin-valley locked band structure, magneto-optical properties under optical pumping of σ^+ (σ^-) circularly polarized light for $B > 0$ are expected to be similar to those under laser excitation with helicity σ^- (σ^+) for $B < 0$.

For avoiding fragmentation of parameters distributed in different sections, in Tables I–V, we summarize the relevant parameters adopted in our calculation, including energy parameters (Table I), valley Zeeman g factors (Table II), excitonic lifetimes (Table III), and intravalley (Table IV) and intervalley (Table V) scattering rates.

B. Peak energy and valley Zeeman splitting for excitons and trions

Before discussing in detail the valley dynamics of excitonic complexes of neutral and charged excitons in monolayer WSe_2, we first determine the peak energies and valley Zeeman effects, which are essential for magneto-optical properties. In Fig. 1(b), we schematically illustrate the valley Zeeman shifts of singlet (X_s^-) and triplet (X_t^-) trions in the K and K' valleys, comprising three contributions from the spin magnetic moment, valley (pseudospin) magnetic moment, and the atomic magnetic moment (Sec. II). It is clear that the valley splitting energy of X_t^- ($6\ \mu_B B$) is three times larger than that of X_s^- ($2\ \mu_B B$), due to distinct spin/valley configurations of the extra electron between singlet and triplet state trions [Fig. 1(a)]. Despite this distinction, the PL peak splitting for X_s^- and X_t^- due to the Zeeman shift is expected to be the same and should be identical to that of excitons, i.e., about $4\ \mu_B B$ [58], as the extra electron in this *trivial* picture contributes identically to both the initial and final-state magnetic moments of the trion, as also illustrated in Fig. 1(b) by the optical emission of σ^+ (red arrow) and σ^- (blue arrow) circularly polarized lights (dichroism paradigm). This intuitive description is in stark contrast to experimental reports [30,58], in which the trion peak splitting is much larger than that of excitons, as we analyze next.

In Fig. 1(c), we show our numerical outcome of excitonic peak energies for singlet and triplet trions in monolayer WSe_2 under both σ^+ (red solid curves) and σ^- (blue solid curves) circularly polarized light fields. The dotted (black) curves represent the peak energies without including the contributions of magnetic moments from the Berry curvature of the initial state (trion) and from the recoil effect of the final state (electron). Thus, they also represent peak energies of neutral excitons. It is found that there exists a great agreement (discrepancy) between solid (dotted) curves and circular markers, which refer to experimental data of Ref. [30], indicating the importance of the trion-fine-structure induced Berry curvature (initial state) and the recoil effect of the extra electron (final state) for trion peak energies.

More specifically, from Eqs. (9)–(11) it is straightforward to obtain the peak energy splitting between σ^+ and σ^- circular polarizations, with $2(\Delta_a + \Delta_b - \Delta_e)$ for X_s^- and $2(\Delta_a + \Delta_b + \Delta_e)$ for X_t^-. Here the first term represents the atomic magnetic contribution, which also refers to the peak energy splitting of neutral excitons; the second term stands for the Berry curvature contribution from the initial-state trion, and the third term describes the recoil effect of the final-state electron. Due to the Berry-curvature contribution, the peak energy splitting for either X_s^- or X_t^- is found greater than that for excitons, consistent with experimental reports [30,58], cf. solid (red and blue) and dotted (black) curves of Fig. 1(c). Moreover, because of the recoil effect of the extra electron, the splitting for X_s^- is greater than that for X_t^-, cf. red and blue (solid) curves of Fig. 1(c). Furthermore, under the laser pumping of circularly polarized light with a given helicity, we also observe that the B-field dependence of peak energies of both singlet and triplet trions have distinct variation rates between $B > 0$ and $B < 0$, which is attributed to the Landau level quantization, see Eqs. (10) and (11).

Figure 3(a) shows the energy separation ($\Delta E_{\rm bd}$) between bright and dark excitons of the same valley (red curves) and the singlet-triplet splitting ($\Delta E_{\rm st}$) between X_s^- and X_t^- of different valleys (green curves). Note that here we focus on the singlet-triplet splitting of different valleys, because it greatly affects thermal equilibrium process of the essential relaxation channel 10, instead of singlet-singlet and triplet-triplet splittings, which plays a negligible role in the trion valley dynamics due to quenched intervalley relaxation of the same trion types (Fig. 2). For the K-valley excitation (red solid curve) under the laser pumping of σ^+ polarization, we find that $\Delta E_{\rm bd}$ grows with increasing magnetic field, primarily due to the spin magnetic moment of electrons in the conduction band. Since the two valleys are *bridged* by time-reversal symmetry, the bright-dark energy separation in the K' valley will exhibit opposite magnetic response (red dotted curve). The singlet-triplet splitting $\Delta E_{\rm st}(B = 0) = \delta_{\rm ex} = 6$ meV determines the fine structure of trions at zero field. When the magnetic field is switched on, we observe that $\Delta E_{\rm st}$ between X_s^- in the K' (K) valley and X_t^- in the K (K') valley tends to be quenched (enhanced) as B increases, see green dotted (solid) curves, following from combined contributions of distinct magnetic moments (Sec. II). From the green dotted (solid) curves for $B > 0$ ($B < 0$), it implies that $\Delta E_{\rm st}$ may vanish for either a larger B field or a less $\delta_{\rm ex}$. These features are helpful for clarifying relevant magneto-optical properties in monolayer WSe_2, which we will discuss later on.

In Fig. 3(b), we show the valley Zeeman splitting $\Delta E_i^{KK'} = E_i^K - E_i^{K'}$, with i representing the excitonic states of X_b, X_s^-, and X_t^- [Eqs. (6)–(8)]. Clearly, the magnitude of $\Delta E_i^{KK'}$, which characterizes the valley degeneracy lifting, increases with growing strength of magnetic field. Our calculation reveals that the associated Landé factors for X_b, X_s^-, and X_t^- are $g_{X_b} = 4$, $g_{X_s^-} = 6$, and $g_{X_t^-} = 10$, respectively. Note that here $\Delta E_i^{KK'}$ only accounts for the initial state (trion), in contrast with the energetic peak splittings between σ^+ and σ^- polarizations shown in Fig. 1(c), which also incorporate the final state (electron) of trions with the corresponding g factors equal to 4, 10.6, and 5.4, respectively, consistent with experimental reports [30]. Clearly, these two descriptions are equivalent for excitons, giving rise to the same g factor equal to four, as there is no extra electron left when the electron-hole pair recombines.

We should emphasize that there exists quite a discrepancy for the trion valley g factors among different experimental reports ranging from 3.9 to 10.5 [30,58,66,68,84–87]. Some of them indicate that the trion g factors are larger than that of excitons [30,58,68,84,85], indicating the importance of the emergent Berry curvature associated with the trion fine structure induced by the exchange interaction. In contrast, there are also experimental measurements showing that the trion and exciton g factors are essentially the same [66,86,87], implying that the contribution from the atomic d orbital of the transition-metal atom dominates the trion valley Zeeman splitting. Moreover, even for the exciton g factors, there are also reports of about $g_{X_b} = 2$ [32], which is essentially half of the widely reported value (4) in the literature, primarily because of the distinct masses between electron and hole. Note that these discrepancies for valley g factors demonstrated in different experiments will not alter the main feature (e.g., X and V shapes) of the magnetic response of excitonic valley polarization, which mainly depends on the fine structure of trions, as we discuss below.

Now, we are ready to analyze our numerical outcome on exciton and trion valley dynamics. We first turn to the magneto-optical properties of neutral excitons.

C. X-shape valley polarization for neutral excitons

Figure 3(c) shows the PL intensity of X_b as a function of magnetic field under laser excitation of both σ^+ and σ^- circularly polarized light fields. It is found that the B-field dependence of PL features an X-type shape. More specifically, for σ^+ (K-valley) excitation and $B > 0$, the optical emissions

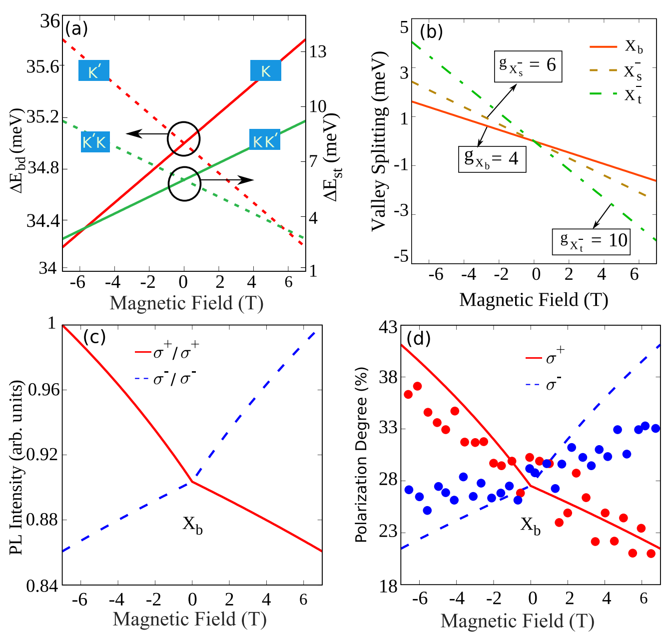

FIG. 3. (a) Left vertical axis: magnetic-field dependence of bright-dark exciton energy separation in the K (solid red line) and K' (dotted red line) valleys; right vertical axis: singlet-triplet trion splittings between X_s^- in the K valley and X_t^- in the K' valley (solid green line, denoted "KK'") and between X_s^- in the K' valley and X_t^- in the K valley (dotted green line, denoted "$K'K$") as functions of magnetic field. (b) Valley Zeeman splitting $\Delta E^{KK'}$ of bright excitons (X_b) and singlet (X_s^-) and triplet (X_t^-) trions as functions of magnetic field. (c) PL intensity and (d) valley polarization of bright excitons for both σ^+ and σ^- excitations as functions of magnetic field. In panel (b), the associated g factors for X_b, X_s^-, and X_t^- are equal to $g_{X_b} = 4$, $g_{X_s^-} = 6$, and $g_{X_t^-} = 10$, respectively. In panel (c), for σ^+ (σ^-) excitation, the PL is detected in co-polarized configurations, implying that the corresponding optical process occurring in the K (K') valley. In panel (d), the markers refer to experimental data of Ref. [6] and the lines are obtained from our theoretical simulation.

become weakened as B increases. Here the quenching PL with increasing B primarily arises from two resources. First, as the magnetic field strengthens, the bright-dark separation ΔE_{bd} in the K valley increases [Fig. 3(a)], in favor of more bright (higher-energy) states relaxing into dark (low-energy) states through the scattering channel 1 (Fig. 2). Second, the field-dependent intervalley scattering time $1/\alpha_{\mathrm{x}}^{KK'}$ [Eq. (17)], which is obtained by fitting exciton and trion VPs to experimental data of Ref. [58] (Sec. III A), decreases with B and further enhances the intervalley scattering of $\mathrm{X_b}$ from K to K' valleys, which is mainly caused by the electron-hole exchange interaction (phonon-assisted scattering) in the absence (presence) of a magnetic field [21,88], leading to the reduction of emission for σ^+ excitation with detection by σ^+ polarization. Considering the magnetic nature of the valley degree of freedom, the X-shape magnetic response of excitons between σ^+ and σ^- excitations follows straightforwardly.

In Fig. 3(d), we show the dependence of exciton VP on magnetic field under both σ^+ and σ^- excitations. Similar to PL, the VP also exhibits an X-shape magnetic dependence on B, agreeing with experimental data of Ref. [58]. Specifically, for σ^+ excitation, the exciton VP weakens when the magnetic field increases, as a direct consequence of decreased intervalley relaxation time [Eq. (17)]. Here we should emphasize two points: First, the discrepancy between our simulated VP and experimental data for σ^- excitation is attributed to the experimental sample itself [58], which features an overall tilt of the X shape; cf. blue and red markers. The reason is as follows: Since the two valleys at zero B field are connected by time-reversal symmetry (i.e., spin-valley locking), the valley Zeeman shifts for the two valleys are opposite while with the same magnitude. Accordingly, the valley polarization under σ^+ excitation for a positive B field is expected to be the same as that under σ^- excitation for a negative B field of the same magnitude. In other words, even though the time-reversal symmetry is broken in the presence of magnetic field, the magneto-optical properties are expected to remain invariant for σ^+ (K-valley) excitation at $B > 0$ and σ^- (K'-valley) excitation at $B < 0$. It is worth noting that the diamagnetic shift (quadratic correction) may also lead to the asymmetry of the X shape, while this high-order effect usually becomes important in the high-field regime [89], which is not the case here. Second, the fitting is made simultaneously for exciton and trion VPs, with the latter also consistent with experimental data [58], as shown in Fig. 4(f) that we will discuss later on, ensuring the validity of our model.

In addition, under the laser excitation of a given helicity we also reveal distinct slopes of the B-field dependence of PL (and VP) between the $B > 0$ and $B < 0$ cases [Figs. 3(c) and 3(d)], resembling the magnetic response of excitonic peak energies [Fig. 1(c)] [30]. Specifically, for σ^+ excitation, the slope of PL with the magnetic field at $B > 0$ is less than that at $B < 0$. This can be understood as follows: When $B > 0$ ($B < 0$), the energy of $\mathrm{X_b}$ in the K valley is lower (higher) than that in the K' valley [Fig. 3(b)], which quenches (reinforces) the thermal process of intervalley scattering of $\mathrm{X_b}$ from the K to K' valleys and accordingly refrains (enhances) the dependence of PL intensity on magnetic field. Thus, different dependence of PL (and VP) on magnetic field for different signs of B follows.

D. X- and V-shape valley polarizations for trions

Now we move to the magneto-optical properties of trions. Experimentally, the measured trion PL and VP are usually superposition of $\mathrm{X_s^-}$ and $\mathrm{X_t^-}$ emissions as their peak energies only have a separation of a few meV [6,30]. Here, our simulation allows us to identify the PL and VP from distinct contributions of $\mathrm{X_s^-}$ and $\mathrm{X_t^-}$. In Figs. 4(a)–4(c), we show the PL intensity of singlet and triplet trions as well as their total emissions, respectively. Since the singlet $\mathrm{X_s^-}$ state has a lower energy than the triplet $\mathrm{X_t^-}$ state, which facilitates the relaxation from the latter to the former (see scattering 10 in Fig. 2), the PL intensity of $\mathrm{X_s^-}$ is found larger than that of $\mathrm{X_t^-}$; cf. Figs. 4(a) and 4(b), consistent with experimental measurements [30]. Below we analyze the magnetic response of trion PLs and VPs in detail.

Similar to neutral excitons, we observe that the B-field dependence of PL intensity of $\mathrm{X_s^-}$ exhibits the X-type shape [Fig. 4(a)], which is mainly attributed to the role of the singlet-triplet scattering channel (see process 10 in Fig. 2). For σ^+

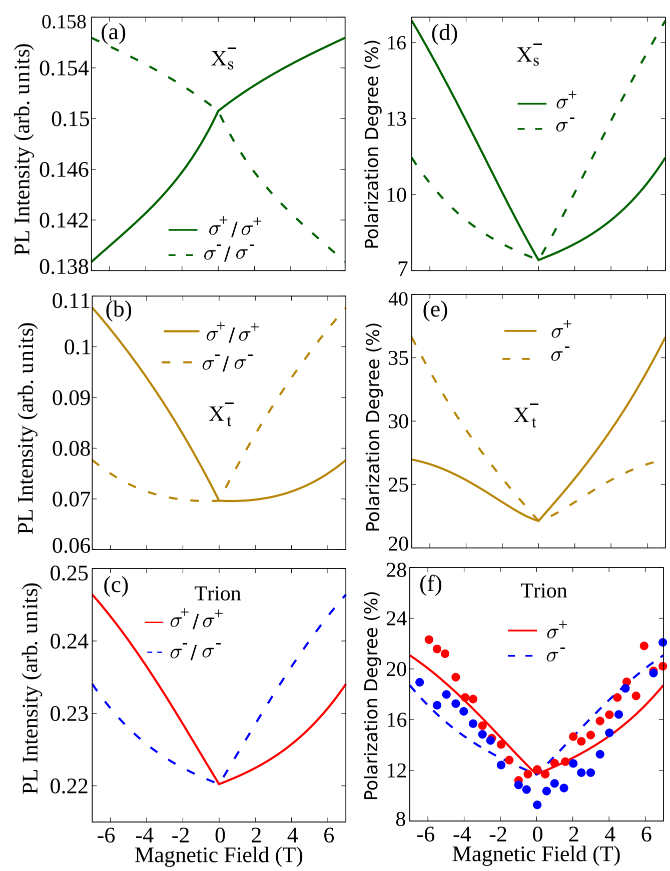

FIG. 4. PL intensity of (a) singlet ($\mathrm{X_s^-}$) and (b) triplet ($\mathrm{X_t^-}$) trions as well as the total PLs of the two trion states (c) as functions of magnetic field, under the laser excitation of σ^+ and σ^- circularly polarized light. For σ^+ (σ^-) excitation, the PL is also detected by σ^+ (σ^-) polarization. (d)–(f) Magnetic-field dependence of the corresponding valley polarizations associated with panels (a)–(c), respectively. In panel (f), the V-shape valley polarization of the total trion emissions including contributions of $\mathrm{X_s^-}$ and $\mathrm{X_t^-}$, with the markers referring to experimental data of Ref. [6] and the lines from our theoretical simulation.

(K-valley) excitation, it is the thermal excitation determining the intervalley scattering of X_s^- to X_t^-, which depends on the energy separation ΔE_{st}. When $B > 0$, ΔE_{st} between X_s^- in the K valley and X_t^- in the K' valley increases with B [Fig. 3(b)]. This suppresses the thermal process of intervalley scattering from X_s^- to X_t^-, giving rise to enhancing X_s^- PL with increasing B for σ^+ excitation. Analogously, when $B < 0$, ΔE_{st} will have opposite dependence on the magnitude of B, as compared with the case of $B > 0$. Thus, for negative B fields the PL intensity of X_s^- under σ^+ excitation decreases with increasing field strength. Considering the optical dichroism characteristic of the two valleys, the X-type shape of PL between σ^+ and σ^- polarizations follows. Note that there also exists distinct slopes under laser excitation of a given helicity between positive and negative fields, similar to those for excitons.

In contrast to X_s^-, the magnetic response of PL for X_t^- features a V-type shape [Fig. 4(b)]. Clearly, the relaxation from X_t^- (higher energy) to X_s^- (lower energy) of distinct valleys are energetically favorable. Thus, it is the combined effect of the field-dependence of the intervalley scattering time $1/\alpha_{st}^{KK'}$ [Eq. (18)] and thermal excitation determining the magneto-optical properties of X_t^-. In the two cases of $B > 0$ and $B < 0$, different variation rates for $1/\alpha_{st}^{KK'}$ as functions of B lead to distinct increasing rates of the PL. As for the total contribution of X_s^- and X_t^- to PL [Fig. 4(c)], the behavior of magnetic response exhibits the V-type shape, dominated by the triplet species. Note that the PL intensity also features nonlinear field dependence, which is attributed to the interplay of multiscattering channels among excitonic states, in particular the intervalley scatterings between singlet trions in the K (K') valley and triplet trions in the K' (K) valley. The involved thermal process, which depends on the fine structure of the trion states, gives rise to the nonlinear part of the trion emissions.

In addition to the singlet-triplet relaxation channel aforementioned, we should emphasize that the nonradiative scattering between X_s^- (X_t^-) and X_d^-, i.e., process 5 (6) of Fig. 2, in general also affects the trion valley dynamics. However, the effect of this latter process on the magnetic response of trion PLs is negligible as compared with the process 10 analyzed above. This is because the bright-dark energy separation $\Delta E_{bd} \approx 35$ meV [78] is much larger than the singlet-triplet splitting $\delta_{ex} = 6$ meV [25], quenching the magnetic effect of the process 5.

Figures 4(d)–4(f) show the corresponding valley polarizations of different trion species referring to Figs. 4(a)–4(c), respectively. We observe that either X_s^- and X_t^- VPs feature an *asymmetric* V shape as functions of magnetic field with respect to $B = 0$. Since the intervalley relaxation of the same type of trions, i.e., singlet-singlet or triplet-triplet scattering, is greatly suppressed (Sec. II), it is the singlet-triplet (intervalley) scattering channel dominating the field dependence of VPs. We first focus on singlet X_s^- state. For σ^+ excitation, the concentration of X_s^- in the K and K' valleys respectively increases and decreases with increasing magnetic field when $B > 0$ [Fig. 4(a)], which is determined by the magnetic response of ΔE_{st}, leading to enhancing VP of X_s^-. On the other hand, when $B < 0$, although the X_s^- concentration in both valleys decreases, while in the K' valley it reduces more abruptly due to quenched intervalley scattering [Eq. (18)], giving rise to an asymmetric V-shape magnetic response of X_s^- across $B = 0$.

For the triplet X_t^- state, we observe that its B-field dependence also exhibits a V-type shape, similar to X_s^-. Remarkably, the VP *asymmetry* between the two trion species may compensate to each other, cf. Figs. 4(d) and 4(e), primarily because the relaxation from X_t^- to X_s^- is energetically favorable while the reversed process is not. This yields a nearly *symmetric* V shape for combined contributions of the two trion species, see Fig. 4(f). Our simulated trion VP is in great agreement with experimental data, cf. curves and markers in Fig. 4(f). As we already mentioned before, the fitting is made simultaneously for exciton and trion VPs, either of which is consistent with experimental measurements [Figs. 3(d) and 4(f)], ensuring the validity of our model.

E. Fine structure mediated new paradigm more than X and V shapes

Since the singlet-triplet intervalley scattering process, which depends on the fine structure of trions, dominates the trion valley dynamics, below we explore the effect of trion fine structure on valley polarization. We demonstrate that the V shape of trion VP is largely tunable. More specifically, when the exchange interaction is reduced, we reveal an X-V shape conversion and even a new paradigm more than the X and V shapes, determined by a *switch* of the ground state for bright trions.

In Figs. 5(a)–5(d), we show the trion VP of total X_s^- and X_t^- emissions, for the zero-field singlet-triplet splitting δ_{ex} equal to 6, 3, 1, and 0.5 meV, respectively. As δ_{ex} decreases, we observe that the V shape tends to transform to the X-like shape; cf. Figs. 5(a)–5(d). Actually, in Figs. 5(c) and 5(d) with smaller values of δ_{ex}, the magnetic response of VP can be divided into two regimes, marked by a critical value of magnetic field B_c (see orange circles) at which the B-field-dependent singlet-triplet splitting vanishes, i.e., $\Delta E_{st}(B = B_c) = 0$. When $|B| \leqslant B_c$, the VP as a function of magnetic field display an X-type shape. Namely, as the strength of magnetic field grows, the trion VP increases and decreases for positive and negative B fields, respectively. On the other hand, when $|B| > B_c$, the field dependence of VP with B is reversed, more than the X- and V-type shapes. Note that in experiment it is feasible to realize a tuning of δ_{ex} by modifying the dielectric environment of WSe_2 monolayer, which varies the exchange interaction. Alternatively, for a given δ_{ex}, one can also resort to ferromagnetic substrate, which gives rise to strong exchange interaction [53,90], for realizing the ground-state switch between singlet and triplet trion states and a further the new paradigm of magnetic response for trions.

Clearly, the valley dynamics of charged excitons depends on the concentration (n_e) of free carriers. Due to screening effect, the free carriers in general may reduce the excitonic binding energy and oscillator strength as well as electron-hole exchange interaction, giving rise to an enhancement of radiative lifetime and valley relaxation time [91,92]. Furthermore, a higher carrier density also favors the conversion of more excitons to trions, suppressing (enhancing) exciton (trion) emissions [54,93,94]. Accordingly, an enhanced valley polarization in principle follows as the free carrier density

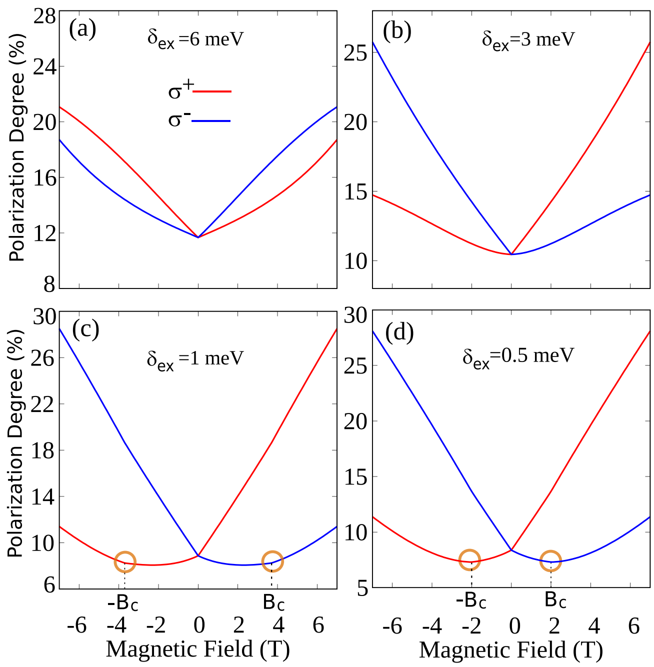

FIG. 5. Valley polarization of the total trion emissions including contributions of X_s^- and X_t^- as functions of magnetic field, for four cases of trion fine structures with (a) $\delta_{ex} = 6$, (b) 3, (c) 1, and (d) 0.5 meV. The orange circles mark where a swap of ground states for bright trions between X_s^- and X_t^- occurs. The monolayer WSe_2 is pumped by laser excitation of σ^+ or σ^- circularly polarized light fields.

increases [54,94]. Despite this, we should emphasize that the general feature of X- and V-type shapes of magnetic response of excitons and trions remains as n_e varies.

It is also worth noting that, in the presence of free carriers, in addition to the bounded three-particle trions, there may also exist other intriguing quasiparticles including exciton polarons (i.e., excitons dressed with a Fermi sea of charges) [95,96] and trion polaritons [97]. And, when the Fermi level is above the conduction-band edge at an even higher carrier density, the trion binding energy may also acquire a term due to state-filling effects [32]. More work is needed to explore these interesting possibilities.

IV. CONCLUDING REMARKS

Considering the lagging theoretical study on magneto-valley dynamics of different trion species in TMDC monolayers, we construct a model which takes into account excitonic states of both bright and dark types, to determine magnetic responses of the PL intensity and the VP degree. To this end, we first compute the excitonic peak energies and valley Zeeman shifts, which are essential for magneto-optical properties. In this process, we account for all relevant contributions to excitonic energy shifts, including the spin magnetic moment, valley (pseudospin) magnetic moment, and orbital magnetic moment as well as the magnetic moment due to the trion-fine-structure associated Berry curvature (initial state) and the recoil effect and Landau-level quantization of the extra electron (final state). Taking monolayer WSe_2 as a model system, our computed peak energy and valley Zeeman splitting for both singlet and triplet trion states are consistent with experiment data by Lyons *et al.* [30], where the Berry-curvature associated magnetic moment enhances the trion peak energy splitting between circular polarizations of distinct helicities and the recoil effect of the extra electron distinguish the peak energy splittings of singlet and triplet trion states. Then, we further determine the PL intensity and the VP degree. We reveal that the exciton and trion VPs respectively exhibit the X- and V-shape dependence on magnetic field, consistent with experimental measurements by Aivazian *et al.* [6]. Furthermore, beyond current experiments, for the trion VP our calculation also indicates an X-V shape conversion and even a new paradigm more than the X and V shapes, depending on the fine structure of trions. Our results are helpful for elucidating recent experimental data about the valley-degeneracy-lifting mediated valley dynamics of different trion species, and should stimulate experiments probing relevant new magneto-optical features.

In our calculation on magneto-optics of TMDCs, we have mainly adopted rate equations, while it is worth noting that from a more microscopic point of view, one can also resort to the semiconductor Bloch equation [42,98–100] for determining the excitonic optical properties. In this procedure, for simplicity it is widely done in the exciton basis by solving the Wannier equation [43,101]. Then, with the help of the Heisenberg equation of motion, the semiconductor Bloch equation, in which the carrier-carrier interaction, carrier-light interaction, and carrier-phonon interaction are also included, can be obtained [42,100,102].

As a final remark, since the valley polarization monotonically depends on magnetic field, a high VP is expected to achieve, e.g., by putting TMDC samples on ferromagnetic substrates [53,90,103], which through exchange interaction provides much stronger magnetization. Also, the proximate effect of TMDCs-ferromagnet van der Waals heterostructures allows us to tailor the electronic band structure of adjacent materials [104–106], offering an ideal platform for manipulating spintronic [107], superconducting [108], excitonic [109], and topological [110] phenomena.

ACKNOWLEDGMENTS

This work was supported by the National Natural Science Foundation of China (Grant No. 11874236), the Major Basic Program of Natural Science Foundation of Shandong Province (Grant No. ZR202105280001), the Research Fund of Qufu Normal University, and the Brazilian funding agencies CNPq, CAPES, and FAPDF. S.X.H. was partially supported by Shandong Provincial Natural Science Foundation (Grant No. ZR2019BA007). We thank L. Liang for critical reading of the whole manuscript.

[1] F. C. Wu, F. Y. Qu, and A. H. MacDonald, Exciton band structure of monolayer MoS_2, Phys. Rev. B **91**, 075310 (2015).

[2] K. F. Mak, K. L. McGill, J. Park, and P. L. McEuen, The valley Hall effect in MoS_2 transistors, Science **344**, 1489 (2014).

[3] F. Y. Qu, A. C. Dias, J. Y. Fu, L. V. Lelovsky, and D. L. Azevedos, Tunable spin and valley dependent magneto-optical absorption in molybdenum disulfide quantum dots, Sci. Rep. **7**, 41044 (2016).

[4] D. Xiao, G. B. Liu, W. X. Feng, X. D. Xu, and W. Yao, Coupled Spin and Valley Physics in Monolayers of MoS_2 and Other Group-VI Dichalcogenides, Phys. Rev. Lett. **108**, 196802 (2012).

[5] K. F. Mak, K. L. He, J. Shan, and T. F. Heinz, Control of valley polarization in monolayer MoS_2 by optical helicity, Nat. Nanotechnol. **7**, 494 (2012).

[6] G. Aivazian, Z. R. Gong, A. M. Jones, R. L. Chu, J. Q. Yan, D. G. Mandrus, C. W. Zhang, D. Cobden, W. Yao, and X. D. Xu, Magnetic control of valley pseudospin in monolayer WSe_2, Nat. Phys. **11**, 148 (2015).

[7] G. Wang, X. Marie, B. L. Liu, T. Amand, C. Robert, F. Cadiz, P. Renucci, and B. Urbaszek, Control of Exciton Valley Coherence in Transition Metal Dichalcogenide Monolayers, Phys. Rev. Lett. **117**, 187401 (2016).

[8] A. M. Jones *et al.*, Optical generation of excitonic valley coherence in monolayer WSe_2, Nat. Nanotechnol. **8**, 634 (2013).

[9] K. Hao, L. X. Xu, F. C. Wu, P. Nagler, K. Tran, X. Ma, C. Schüller, T. Korn, A. H. MacDonald, G. Moody, and X. Q. Li, Trion valley coherence in monolayer semiconductors, 2D Mater. **4**, 025105 (2017).

[10] K. Hao, G. Moody, F. C. Wu, C. K. Dass, L. X. Xu, C. H. Chen, L. Y. Sun, M. Y. Li, L. J. Li, A. H. MacDonald, and X. Q. Li, Direct measurement of exciton valley coherence in monolayer WSe_2, Nat. Phys. **12**, 677 (2016).

[11] S. Mouri, Y. Miyauchi, M. Toh, W. Zhao, G. Eda, and K. Matsuda, Nonlinear photoluminescence in atomically thin layered WSe_2 arising from diffusion-assisted exciton-exciton annihilation, Phys. Rev. B **90**, 155449 (2014).

[12] A. C. Dias, J. Y. Fu, L. V. Lelovsky, and F. Y. Qu, Robust effective Zeeman energy in monolayer MoS_2 quantum dots, J. Phys.: Condens. Matter **28**, 375803 (2016).

[13] C. Robert, D. Lagarde, F. Cadiz, G. Wang, B. Lassagne, T. Amand, A. Balocchi, P. Renucci, S. Tongay, B. Urbaszek, and X. Marie, Exciton radiative lifetime in transition metal dichalcogenide monolayers, Phys. Rev. B **93**, 205423 (2016).

[14] G. Plechinger, P. Nagler, A. Arora, R. Schmidt, A. Chernikov, A. Granados del Águila, P. C. M. Christianen, R. Bratschitsch, C. Schüller, and T. Korn, Trion fine structure and coupled spin-valley dynamics in monolayer tungsten disulfide, Nat. Commun. **7**, 12715 (2016).

[15] T. Godde, D. Schmidt, J. Schmutzler, M. Aßmann, J. Debus, F. Withers, E. M. Alexeev, O. D. Pozo-Zamudio, O. V. Skrypka, K. S. Novoselov, M. Bayer, and A. I. Tartakovskii, Exciton and trion dynamics in atomically thin $MoSe_2$ and WSe_2: Effect of localization, Phys. Rev. B **94**, 165301 (2016).

[16] F. Gao, Y. J. Gong, M. Titze, R. Almeida, P. M. Ajayan, and H. B. Li, Valley trion dynamics in monolayer $MoSe_2$, Phys. Rev. B **94**, 245413 (2016).

[17] K. L. He, N. Kumar, L. Zhao, Z. F. Wang, K. F. Mak, H. Zhao, and J. Shan, Tightly Bound Excitons in Monolayer WSe_2, Phys. Rev. Lett. **113**, 026803 (2014).

[18] E. Courtade, M. Semina, M. Manca, M. M. Glazov, C. Robert, F. Cadiz, G. Wang, T. Taniguchi, K. Watanabe, M. Pierre, W. Escoffier, E. L. Ivchenko, P. Renucci, X. Marie, T. Amand, and B. Urbaszek, Charged excitons in monolayer WSe_2: Experiment and theory, Phys. Rev. B **96**, 085302 (2017).

[19] H. Y. Yu, X. D. Cui, X. D. Xu, and W. Yao, Valley excitons in two-dimensional semiconductors, Natl. Sci. Rev. **2**, 57 (2015).

[20] H. Y. Yu, G. B. Liu, P. Gong, X. D. Xu, and W. Yao, Dirac cones and Dirac saddle points of bright excitons in monolayer transition metal dichalcogenides, Nat. Commun. **5**, 3876 (2014).

[21] T. Yu and M. W. Wu, Valley depolarization due to intervalley and intravalley electron-hole exchange interactions in monolayer MoS_2, Phys. Rev. B **89**, 205303 (2014).

[22] M. Baranowski, A. Surrente, D. K. Maude, M. Ballottin, A. A. Mitioglu, P. C. M. Christianen, Y. C. Kung, D. Dumcenco, A. Kis, and P. Plochocka, Dark excitons and the elusive valley polarization in transition metal dichalcogenides, 2D Mater. **4**, 025016 (2017).

[23] J. P. Echeverry, B. Urbaszek, T. Amand, X. Marie, and I. C. Gerber, Splitting between bright and dark excitons in transition metal dichalcogenide monolayers, Phys. Rev. B **93**, 121107(R) (2016).

[24] F. Volmer, S. Pissinger, M. Ersfeld, S. Kuhlen, C. Stampfer, and B. Beschoten, Intervalley dark trion states with spin lifetimes of 150 ns in WSe_2, Phys. Rev. B **95**, 235408 (2017).

[25] J. Y. Fu, J. M. R. Cruz, and F. Y. Qu, Valley dynamics of different trion species in monolayer WSe_2, Appl. Phys. Lett. **115**, 082101 (2019).

[26] Z. P. Li, T. M. Wang, Z. G. Lu, M. Khatoniar, Z. Lian, Y. Z. Meng, M. Blei, T. Taniguchi, K. Watanabe, S. McGill, S. A. Tongay, V. M. Menon, D. Smirnov, and S. F. Shi, Direct observation of gate-tunable dark trions in monolayer WSe_2, Nano Lett. **19**, 6886 (2019).

[27] X. X. Zhang, Y. M. You, S. Y. F. Zhao, and T. F. Heinz, Experimental Evidence for Dark Excitons in Monolayer WSe_2, Phys. Rev. Lett. **115**, 257403 (2015).

[28] A. Hichri and S. Jaziri, Trion fine structure and anomalous Hall effect in monolayer transition metal dichalcogenides, Phys. Rev. B **102**, 085407 (2020).

[29] A. Singh, K. Tran, M. Kolarczik, J. Seifert, Y. P. Wang, K. Hao, D. Pleskot, N. M. Gabor, S. Helmrich, N. Owschimikow, U. Woggon, and X. Q. Li, Long-Lived Valley Polarization of Intravalley Trions in Monolayer WSe_2, Phys. Rev. Lett. **117**, 257402 (2016).

[30] T. Lyons, S. Dufferwiel, M. Brooks, F. Withers, T. Taniguchi, K. Watanabe, K. S. Novoselov, G. Burkard, and A. I. Tartakovskii, The valley Zeeman effect in inter- and intravalley trions in monolayer WSe_2, Nat. Commun. **10**, 2330 (2019).

[31] P. Kapuściński, D. Vaclavkova, M. Grzeszczyk, A. O. Slobodeniuk, K. Nogajewski, M. Bartos, K. Watanabe, T. Taniguchi, C. Faugeras, A. Babiński, M. Potemski, and M. R. Molas, Valley polarization of singlet and triplet trions in a WS_2 monolayer in magnetic fields, Phys. Chem. Chem. Phys. **22**, 19155 (2020).

[32] Y. Li, J. Ludwig, T. Low, A. Chernikov, X. Cui, G. Arefe, Y. D. Kim, A. M. van der Zande, A. Rigosi, H. M. Hill, S. H. Kim, J. Hone, Z. Q. Li, D. Smirnov, and T. F. Heinz, Valley Splitting and Polarization by the Zeeman Effect in Monolayer $MoSe_2$, Phys. Rev. Lett. **113**, 266804 (2014).

[33] Y. Zhang, K. Shinokita, K. Watanabe, T. Taniguchi, Y. Miyauchi, and K. Matsuda, Magnetic Field Induced Inter-

Valley Trion Dynamics in Monolayer 2D Semiconductor, Adv. Funct. Mater. **31**, 2006064 (2021).

[34] Q. H. Wang, K. Kalantar-Zadeh, A. Kis, J. N. Coleman, and M. S. Strano, Electronics and optoelectronics of two-dimensional transition metal dichalcogenides, Nat. Nanotechnol. **7**, 699 (2012).

[35] K. Kośmider, J. W. González, and J. Fernández-Rossier, Large spin splitting in the conduction band of transition metal dichalcogenide monolayers, Phys. Rev. B **88**, 245436 (2013).

[36] Z. Y. Zhu, Y. C. Cheng, and U. Schwingenschlögl, Giant spin-orbit-induced spin splitting in two-dimensional transition-metal dichalcogenide semiconductors, Phys. Rev. B **84**, 153402 (2011).

[37] X. Chen, T. F. Yan, B. R. Zhu, S. Y. Yang, and X. D. Cui, Optical control of spin polarization in monolayer transition metal dichalcogenides, ACS Nano **11**, 1581 (2017).

[38] J. Y. Fu, A. Bezerra, and F. Y. Qu, Valley dynamics of intravalley and intervalley multiexcitonic states in monolayer WS_2, Phys. Rev. B **97**, 115425 (2018).

[39] T. Deilmann and K. S. Thygesen, Dark excitations in monolayer transition metal dichalcogenides, Phys. Rev. B **96**, 201113(R) (2017).

[40] M. R. Molas, C. Faugeras, A. O. Slobodeniuk, K. Nogajewski, M. Bartos, D. M. Basko, and M. Potemski, Brightening of dark excitons in monolayers of semiconducting transition metal dichalcogenides, 2D Mater. **4**, 021003 (2017).

[41] X. X. Zhang, T. Cao, Z. G. Lu, Y. C. Lin, F. Zhang, Y. Wang, Z. Q. Li, J. C. Hone, J. A. Robinson, D. Smirnov, S. G. Louie, and T. F. Heinz, Magnetic brightening and control of dark excitons in monolayer WSe_2, Nat. Nanotechnol. **12**, 883 (2017).

[42] M. Berghäuser, P. Steinleitner, P. Merkl, R. Huber, A. Knorr, and E. Malic, Mapping of the dark exciton landscape in transition metal dichalcogenides, Phys. Rev. B **98**, 020301(R) (2018).

[43] E. Malic, M. Selig, M. Feierabend, S. Brem, D. Christiansen, F. Wendler, A. Knorr, and G. Berghaüser, Dark excitons in transition metal dichalcogenides, Phys. Rev. Materials **2**, 014002 (2018).

[44] E. Liu, J. van Baren, Z. Lu, M. M. Altaiary, T. Taniguchi, K. Watanabe, D. Smirnov, and C. H. Lui, Gate Tunable Dark Trions in Monolayer WSe_2, Phys. Rev. Lett. **123**, 027401 (2019).

[45] M. H. Zhang, J. Y. Fu, A. C. Dias, and F. Y. Qu, Optically dark excitonic states mediated exciton and biexciton valley dynamics in monolayer WSe_2, J. Phys.: Condens. Matter **30**, 265502 (2018).

[46] T. Smoleński, M. Goryca, M. Koperski, C. Faugeras, T. Kazimierczuk, A. Bogucki, K. Nogajewski, P. Kossacki, and M. Potemski, Tuning Valley Polarization in a WSe_2 Monolayer with a Tiny Magnetic Field, Phys. Rev. X **6**, 021024 (2016).

[47] R. Vasconcelos, H. Braganca, F. Y. Qu, and J. Y. Fu, Dark exciton brightening and its engaged valley dynamics in monolayer WSe_2, Phys. Rev. B **98**, 195302 (2018).

[48] R. Tempelaar and T. C. Berkelbach, Many-body simulation of two-dimensional electronic spectroscopy of excitons and trions in monolayer transition metal dichalcogenides, Nat. Commun. **10**, 3419 (2019).

[49] G. Wang, A. Chernikov, M. M. Glazov, T. F. Heinz, X. Marie, T. Amand, and B. Urbaszek, Colloquium: Excitons in atomically thin transition metal dichalcogenides, Rev. Mod. Phys. **90**, 021001 (2018).

[50] X. Jiang, Q. Zheng, Z. Lan, W. A. Saidi, X. Ren, and J. Zhao, Real-time GW-BSE investigations on spin-valley exciton dynamics in monolayer transition metal dichalcogenide, Sci. Adv. **7**, 3759 (2021).

[51] G. Peng, P. Lo, W. Li, Y. Huang, Y. Chen, C. Lee, C. Yang, and S. Cheng, Distinctive signatures of the spin- and momentum-forbidden dark exciton states in the photoluminescence of strained WSe_2 monolayers under thermalization, Nano Lett. **19**, 2299 (2019).

[52] A. C. Dias, F. Y. Qu, D. L. Azevedo, and J. Y. Fu, Band structure of monolayer transition-metal dichalcogenides and topological properties of their nanoribbons: Next-nearest-neighbor hopping, Phys. Rev. B **98**, 075202 (2018).

[53] A. C. Dias, H. Braganca, H. Zeng, A. L. A. Fonseca, D. S. Liu, and F. Y. Qu, Large room-temperature valley polarization by valley-selective switching of exciton ground state, Phys. Rev. B **101**, 085406 (2020).

[54] F. Riche, H. Braganca, F. Y. Qu, V. Lopez-Richard, S. J. Xie, A. C. Dias, and G. E. Marques, Robust room temperature emissions of trion in darkish WSe_2 monolayers: Effects of dark neutral and charged excitonic states, J. Phys.: Condens. Matter **32**, 365702 (2020).

[55] G. Wang, X. Marie, I. Gerber, T. Amand, D. Lagarde, L. Bouet, M. Vidal, A. Balocchi, and B. Urbaszek, Giant Enhancement of the Optical Second-Harmonic Emission of WSe_2 Monolayers by Laser Excitation at Exciton Resonances, Phys. Rev. Lett. **114**, 097403 (2015).

[56] C. Zhang, Y. Chen, A. Johnson, M. Li, L. Li, P. C. Mende, R. M. Feenstra, and C. Shih, Probing critical point energies of transition metal dichalcogenides: Surprising indirect gap of single layer WSe_2, Nano Lett. **15**, 6494 (2015).

[57] D. K. Zhang, D. W. Kidd, and K. Varga, Excited biexcitons in transition metal dichalcogenides, Nano Lett. **15**, 7002 (2015).

[58] A. Srivastava, M. Sidler, A. V. Allain, D. S. Lembke, A. Kis, and A. Imamoglu, Valley Zeeman effect in elementary optical excitations of monolayer WSe_2, Nat. Phys. **11**, 141 (2015).

[59] W. Feng, Y. Yao, W. Zhu, J. Zhou, W. Yao, and D. Xiao, Intrinsic spin Hall effect in monolayers of group-VI dichalcogenides: A first-principles study, Phys. Rev. B **86**, 165108 (2012).

[60] W. Liu, C. Luo, X. Tang, X. Peng, and J. Zhong, Valleytronic properties of monolayer WSe_2 in external magnetic field, AIP Adv. **9**, 045222 (2019).

[61] M. Van der Donck, M. Zarenia, and F. M. Peeters, Strong valley Zeeman effect of dark excitons in monolayer transition metal dichalcogenides in a tilted magnetic field, Phys. Rev. B **97**, 081109(R) (2018).

[62] M. Koperski, M. R. Molas, A. Arora, K. Nogajewski, M. Bartos, J. Wyzula, D. Vaclavkova, P. Kossacki, and M. Potemski, Orbital, spin and valley contributions to Zeeman splitting of excitonic resonances in $MoSe_2$, WSe_2 and WS_2 monolayers, 2D Mater. **6**, 015001 (2019).

[63] T. Deilmann, P. Krüger, and M. Rohlfing, *Ab Initio* Studies of Exciton *g* Factors: Monolayer Transition Metal Dichalcogenides in Magnetic Fields, Phys. Rev. Lett. **124**, 226402 (2020).

[64] T. Woźniak, P. E. Faria Junior, G. Seifert, A. Chaves, and J. Kunstmann, Exciton g factors of van der Waals heterostructures from first-principles calculations, Phys. Rev. B **101**, 235408 (2020).

[65] F. Xuan and S. Y. Quek, Valley Zeeman effect and Landau levels in two-dimensional transition metal dichalcogenides, Phys. Rev. Research **2**, 033256 (2020).

[66] J. Förste, N. V. Tepliakov, S. Y. Kruchinin, J. Lindlau, V. Funk, M. Förg, K. Watanabe, T. Taniguchi, A. S. Baimuratov, and A. Högele, Exciton g-factors in monolayer and bilayer WSe_2 from experiment and theory, Nat. Commun. **11**, 4539 (2020).

[67] C. Robert, H. Dery, L. Ren, D. Van Tuan, E. Courtade, M. Yang, B. Urbaszek, D. Lagarde, K. Watanabe, T. Taniguchi, T. Amand, and X. Marie, Measurement of Conduction and Valence Bands g-Factors in a Transition Metal Dichalcogenide Monolayer, Phys. Rev. Lett. **126**, 067403 (2021).

[68] M. Zinkiewicz, T. Woźniak, T. Kazimierczuk, P. Kapuscinski, K. Oreszczuk, M. Grzeszczyk, M. Bartoš, K. Nogajewski, K. Watanabe, T. Taniguchi, C. Faugeras, P. Kossacki, M. Potemski, A. Babiński, and M. R. Molas, Excitonic complexes in n-doped WS_2 monolayer, Nano Lett. **21**, 2519 (2021).

[69] The right panel illustrates scattering channels in the K' valley.

[70] M. Z. Maialle, E. A. de Andrada e Silva, and L. J. Sham, Exciton spin dynamics in quantum wells, Phys. Rev. B **47**, 15776 (1993).

[71] A. Vinattieri, J. Shah, T. C. Damen, D. S. Kim, L. N. Pfeiffer, M. Z. Maialle, and L. J. Sham, Exciton dynamics in GaAs quantum wells under resonant excitation, Phys. Rev. B **50**, 10868 (1994).

[72] K. Shinokita, X. F. Wang, Y. H. Miyauchi, K. Watanabe, T. Taniguchi, S. Konabe, and K. Matsuda, Ultrafast dynamics of bright and dark positive trions for valley polarization in monolayer WSe_2, Phys. Rev. B **99**, 245307 (2019).

[73] T. Schmidt, K. Lischka, and W. Zulehner, Excitation-power dependence of the near-band-edge photoluminescence of semiconductors, Phys. Rev. B **45**, 8989 (1992).

[74] P. K. Nayak, F. C. Lin, C. H. Yeh, J. S. Huang, and P. W. Chiu, Robust room temperature valley polarization in monolayer and bilayer WS_2, Nanoscale **8**, 6035 (2016).

[75] Strictly speaking, it is hard to directly distinguish PL spectra of the two valleys. We define the excitonic valley polarization through the distinction of PL between the two valleys as a result of PL intensity proportional to the corresponding excitonic concentrations.

[76] G. Moody, J. Schaibley, and X. D. Xu, Exciton dynamics in monolayer transition metal dichalcogenides, J. Opt. Soc. Am. B **33**, C39 (2016).

[77] Y. You, X. X. Zhang, T. C. Berkelbach, and T. F. Heinz, Observation of biexcitons in monolayer WSe_2, Nat. Phys. **11**, 477 (2015).

[78] K. F. Mak and J. Shan, Photonics and optoelectronics of 2D semiconductor transition metal dichalcogenides, Nat. Photonics **10**, 216 (2016).

[79] M. Yankowitz, D. McKenzie, and B. J. LeRoy, Local Spectroscopic Characterization of Spin and Layer Polarization in WSe_2, Phys. Rev. Lett. **115**, 136803 (2015).

[80] T. C. Berkelbach, M. S. Hybertsen, and D. R. Reichman, Theory of neutral and charged excitons in monolayer transition metal dichalcogenides, Phys. Rev. B **88**, 045318 (2013).

[81] C. Robert, T. Amand, F. Cadiz, D. Lagarde, E. Courtade, M. Manca, T. Taniguchi, K. Watanabe, B. Urbaszek, and X. Marie, Fine structure and lifetime of dark excitons in transition metal dichalcogenide monolayers, Phys. Rev. B **96**, 155423 (2017).

[82] M. T. Portella-Oberli, J. Berney, L. Kappei, F. Morier-Genoud, J. Szczytko, and B. Deveaud-Plédran, Dynamics of Trion Formation in $In_xGa_{1-x}As$ Quantum Wells, Phys. Rev. Lett. **102**, 096402 (2009).

[83] N. Lundt, E. Cherotchenko, O. Iff, X. Fan, Y. Shen, P. Bigenwald, A. V. Kavokin, S. Hofling, and C. Schneide, The interplay between excitons and trions in a monolayer of $MoSe_2$, Appl. Phys. Lett. **112**, 031107 (2018).

[84] G. Wang, L. Bouet, M. M. Glazov, T. Amand, E. L. Ivchenko, E. Palleau, X. Marie, and B. Urbaszek, Magneto-optics in transition metal diselenide monolayers, 2D Mater. **2**, 034002 (2015).

[85] Z. P. Li, T. M. Wang, S. M. Miao, Z. Lian, and S. F. Shi, Fine structures of valley-polarized excitonic states in monolayer transitional metal dichalcogenides, Nanophotonics **9**, 1811 (2020).

[86] D. MacNeill, C. Heikes, K. F. Mak, Z. Anderson, A. Kormányos, V. Zólyomi, J. Park, and D. C. Ralph, Breaking of Valley Degeneracy by Magnetic Field in Monolayer $MoSe_2$, Phys. Rev. Lett. **114**, 037401 (2015).

[87] C. J. Zou, C. X. Cong, J. Z. Shang, C. Zhao, M. Eginligil, L. S. Wu, Y. Chen, H. B. Zhang, S. Feng, J. Zhang, H. Zeng, W. Huang, and T. Yu, Probing magnetic-proximity-effect enlarged valley splitting in monolayer WSe_2 by photoluminescence, Nano Res. **11**, 6252 (2018).

[88] G. Kioseoglou, A. T. Hanbicki, M. Currie, A. L. Friedman, D. Gunlycke, and B. T. Jonker, Valley polarization and intervalley scattering in monolayer MoS_2, Appl. Phys. Lett. **101**, 221907 (2012).

[89] V. Stier, K. M. McCreary, B. T. Jonker, J. Kono, and S. A. Crooker, Exciton diamagnetic shifts and valley Zeeman effects in monolayer WS_2 and MoS_2 to 65 Tesla, Nat. Commun. **7**, 106403 (2016).

[90] T. Norden, C. Zhao, P. Y. Zhang, R. Sabirianov, A. Petrou, and H. Zeng, Giant valley splitting in monolayer WS_2 by magnetic proximity effect, Nat. Commun. **10**, 4163 (2019).

[91] H. N. Wang, C. J. Zhang, W. Chan, C. Manolatou, S. Tiwari, and F. Rana, Radiative lifetimes of excitons and trions in monolayers of the metal dichalcogenide MoS_2, Phys. Rev. B **93**, 045407 (2016).

[92] M. M. Glazov and A. Chernikov, Breakdown of the static approximation for free carrier screening of excitons in monolayer semiconductors, Phys. Status Solidi B **255**, 1800216 (2018).

[93] J. J. Carmiggelt, M. Borst, and T. van der Sar, Exciton-to-trion conversion as a control mechanism for valley polarization in room-temperature monolayer WS_2, Sci. Rep. **10**, 17389 (2020).

[94] Y. Tao, X. Yu, J. Li, H. Liang, Y. Zhang, W. Huang, and Q. J. Wang, Bright monolayer tungsten disulfide via exciton and trion chemical modulations, Nanoscale **10**, 6294 (2018).

[95] T. Goldstein, Y.-C. Wu, S. Chen, T. Taniguchi, K. Watanabe, K. Varga, and J. Yan, Ground and excited state exciton polarons in monolayer $MoSe_2$, J. Chem. Phys. **153**, 071101 (2020).

[96] D. K. Efimkin and A. H. MacDonald, Many-body theory of trion absorption features in two-dimensional semiconductors, Phys. Rev. B **95**, 035417 (2017).

[97] R. P. A. Emmanuele, M. Sich, O. Kyriienko, V. Shahnazaryan, F. Withers, A. Catanzaro, P. M. Walker, F. A. Benimetskiy, M. S. Skolnick, A. I. Tartakovskii, I. A. Shelykh, and D. N. Krizhanovskii, Highly nonlinear trion-polaritons in a monolayer semiconductor, Nat. Commun. **11**, 3589 (2020).

[98] R. Buschlinger, M. Lorke, and U. Peschel, Light-matter interaction and lasing in semiconductor nanowires: A combined finite-difference time-domain and semiconductor Bloch equation approach, Phys. Rev. B **91**, 045203 (2015).

[99] L. Yue and M. B. Gaarde, Structure gauges and laser gauges for the semiconductor Bloch equations in high-order harmonic generation in solids, Phys. Rev. A **101**, 053411 (2020).

[100] M. Feierabend, G. Berghaäuser, A. Knorr, and E. Malic, Proposal for dark exciton based chemical sensors, Nat. Commun. **8**, 14776 (2017).

[101] M. Selig, G. Berghäuser, A. Raja, P. Nagler, C. Schuüller, T. F. Heinz, T. Korn, A. Chernikov, E. Malic, and A. Knorr, Excitonic linewidth and coherence lifetime in monolayer transition metal dichalcogenides, Nat. Commun. **7**, 13279 (2016).

[102] G. Berghäuser and E. Malic, Analytical approach to excitonic properties of MoS_2, Phys. Rev. B **89**, 125309 (2014).

[103] H. Braganca, H. Zeng, A. C. Dias, J. H. Correa, and F. Y. Qu, Magnetic-gateable valley exciton emission, npj Comput. Mater. **6**, 90 (2020).

[104] D. Zhong, K. L. Seyler, X. Linpeng, R. Cheng, N. Sivadas, B. Huang, E. Schmidgall, T. Taniguchi, K. Watanabe, M. A. McGuire, W. Yao, D. Xiao, K.-M. C. Fu, and X. D. Xu, Van der Waals engineering of ferromagnetic semiconductor heterostructures for spin and valleytronics, Sci. Adv. **3**, e1603113 (2017).

[105] K. Zollner, P. E. Faria Junior, and J. Fabian, Proximity exchange effects in $MoSe_2$ and WSe_2 heterostructures with CrI_3: Twist angle, layer, and gate dependence, Phys. Rev. B **100**, 085128 (2019).

[106] D. Zhong, K. L. Seyler, X. Linpeng, N. P. Wilson, T. Taniguchi, K. Watanabe, M. A. McGuire, K.-M. C. Fu, D. Xiao, W. Yao, and X. D. Xu, Layer-resolved magnetic proximity effect in van der Waals heterostructures, Nat. Nanotechnol. **15**, 187 (2020).

[107] I. Vobornik, U. Manju, J. Fujii, F. Borgatti, P. Torelli, D. Krizmancic, Y. S. Hor, R. J. Cava, and G. Panaccione, Magnetic proximity effect as a pathway to spintronic applications of topological insulators, Nano Lett. **11**, 4079 (2011).

[108] A. I. Buzdin, Proximity effects in superconductor-ferromagnet heterostructures, Rev. Mod. Phys. **77**, 935 (2005).

[109] B. Scharf, G. F. Xu, A. Matos-Abiague, and I. Zutić, Magnetic Proximity Effects in Transition-Metal Dichalcogenides: Converting Excitons, Phys. Rev. Lett. **119**, 127403 (2017).

[110] G. Koren, Magnetic proximity effect of a topological insulator and a ferromagnet in thin-film bilayers of $Bi_{0.5}Sb_{1.5}Te_3$ and $SrRuO_3$, Phys. Rev. B **97**, 054405 (2018).